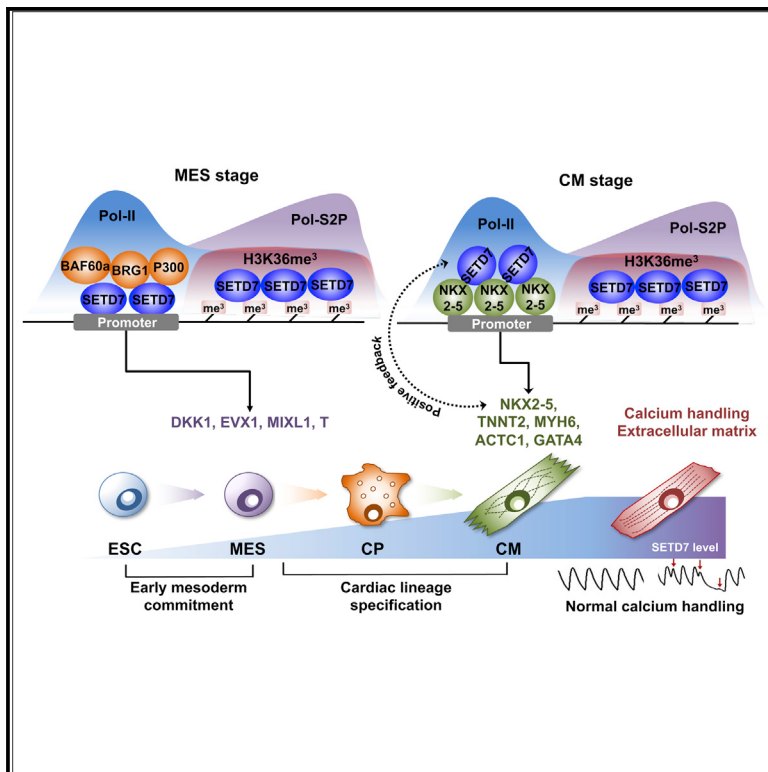


SETD7 Drives Cardiac Lineage Commitment through Stage-Specific Transcriptional Activation

Graphical Abstract



Authors

Jaecheol Lee, Ning-Yi Shao,
David T. Paik, ..., Ioannis Karakikes,
Michael P. Snyder, Joseph C. Wu

Correspondence

joewu@stanford.edu

In Brief

Wu and colleagues define SETD7 as a key regulator of cardiac lineage commitment. SETD7 regulates the expression of lineage-specific target genes and interacts with various co-factors during cardiomyocyte differentiation. SETD7 associates with H3K36me3 histone modification, which is required for the transcriptional activation.

Highlights

- SETD7 targets distinct gene sets at discrete stages of cardiomyocyte specification
- SETD7 interacts with diverse co-factors during cardiomyocyte differentiation
- SETD7 reads H3K36me3 on gene bodies
- SETD7 is required for calcium handling in terminally differentiated cardiomyocytes



SETD7 Drives Cardiac Lineage Commitment through Stage-Specific Transcriptional Activation

Jaecheol Lee,^{1,2,3,9} Ning-Yi Shao,^{1,2,3,9} David T. Paik,^{1,2,3} Haodi Wu,^{1,2,3} Hongchao Guo,^{1,2,3} Vittavat Termglinchan,^{1,2,3} Jared M. Churko,^{1,2,3} Youngkyun Kim,^{1,2,3} Tomoya Kitani,^{1,2,3} Ming-Tao Zhao,^{1,2,3} Yue Zhang,^{4,5} Kitchener D. Wilson,^{1,6} Ioannis Karakikes,^{1,7} Michael P. Snyder,^{1,5,8} and Joseph C. Wu^{1,2,3,10,*}

¹Stanford Cardiovascular Institute, Stanford University School of Medicine, Stanford, CA 94305, USA

²Institute for Stem Cell Biology and Regenerative Medicine, Stanford University School of Medicine, Stanford, CA 94305, USA

³Department of Medicine, Division of Cardiology, Stanford University School of Medicine, Stanford, CA 94305, USA

⁴Genetics Bioinformatics Service Center, Stanford University School of Medicine, Stanford, CA 94305, USA

⁵Department of Genetics, Stanford University School of Medicine, Stanford, CA 94305, USA

⁶Department of Pathology, Stanford University School of Medicine, Stanford, CA 94305, USA

⁷Department of Cardiothoracic Surgery, Stanford University School of Medicine, Stanford, CA 94305, USA

⁸Stanford Center for Genomics and Personalized Medicine, Stanford University School of Medicine, Stanford, CA 94305, USA

⁹These authors contributed equally

¹⁰Lead Contact

*Correspondence: joewu@stanford.edu

<https://doi.org/10.1016/j.stem.2018.02.005>

SUMMARY

Cardiac development requires coordinated and large-scale rearrangements of the epigenome. The roles and precise mechanisms through which specific epigenetic modifying enzymes control cardiac lineage specification, however, remain unclear. Here we show that the H3K4 methyltransferase SETD7 controls cardiac differentiation by reading H3K36 marks independently of its enzymatic activity. Through chromatin immunoprecipitation sequencing (ChIP-seq), we found that SETD7 targets distinct sets of genes to drive their stage-specific expression during cardiomyocyte differentiation. SETD7 associates with different co-factors at these stages, including SWI/SNF chromatin-remodeling factors during mesodermal formation and the transcription factor NKX2.5 in cardiac progenitors to drive their differentiation. Further analyses revealed that SETD7 binds methylated H3K36 in the bodies of its target genes to facilitate RNA polymerase II (Pol II)-dependent transcription. Moreover, abnormal SETD7 expression impairs functional attributes of terminally differentiated cardiomyocytes. Together, these results reveal how SETD7 acts at sequential steps in cardiac lineage commitment, and they provide insights into crosstalk between dynamic epigenetic marks and chromatin-modifying enzymes.

INTRODUCTION

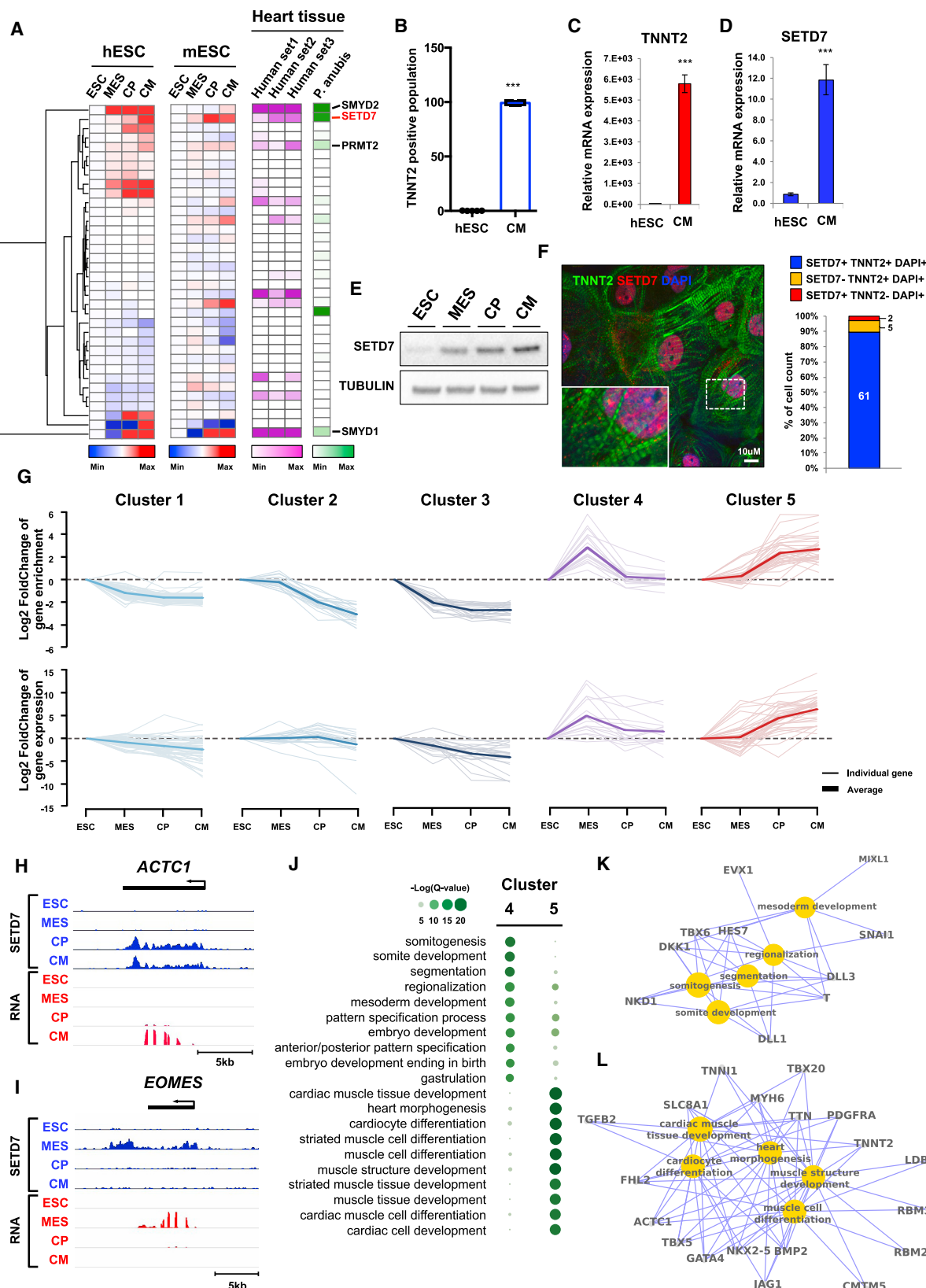
Generation of cardiomyocytes (CMs) from human embryonic stem cells (ESCs) and induced pluripotent stem cells (iPSCs) has emerged as the state-of-the-art approach to study human

cardiac development and pathobiology of adult and congenital heart disease. Cardiac differentiation is regulated by temporal expression of genes critical for mesodermal and cardiac lineage specification, which we modulate *in vitro* to efficiently differentiate human ESCs and iPSCs to functional CMs (Burridge et al., 2012, 2015). In addition, recent studies have demonstrated that coordinated transition of epigenetic modifications is required for stage-specific gene expression during cardiac differentiation (Paige et al., 2012; Wamstad et al., 2012). Genome-wide profiling of active histone markers (H3K4me3 and H3K36me3) and repressive histone marker (H3K27me3) revealed the expression of key regulators for CM differentiation is associated with the transition between H3K4me3 and H3K27me3, whereas the cardiac structural genes showed changes only in H3K4me3. By contrast, the H3K36me3 marker was enriched in both regulatory and cardiac structural genes during the entire duration of CM differentiation.

Epigenetic modifying enzymes play a critical role in epigenetic regulation, with important clinical implications. Recent studies showed impaired function of epigenetic modifying enzymes contributes to congenital heart disease (Chang and Bruneau, 2012; Vallaster et al., 2012), such as in morphological heart defects caused by the loss of H3K36 methyltransferase WHSC1 (Nimura et al., 2009). Mutation in histone methyltransferase MLL2 leads to congenital heart defects in Kabuki syndrome (Ng et al., 2010), and the deficiency of SMYD1 expression during heart development induces malformation of the right ventricle (Li et al., 2013). Chromatin-remodeling factors, such as the SWI/SNF complex, are also critical for early heart development by controlling transcription of cardiac-specific genes (Hang et al., 2010). While these studies provide robust evidence that epigenetic modifying enzymes are essential for normal heart development, the mechanisms by which the epigenetic modifying enzymes regulate the complex gene expression networks of cardiac differentiation through a coordinated transition of epigenetic modifications remain poorly understood.

SETD7 was originally identified as a methyltransferase for histone 3 (H3) lysine 4 residue by mediating mono-methylation





(legend on next page)

(H3K4me1) (Wang et al., 2001). SETD7 diminished its activity for histone assembled in nucleosome but showed high activity with free histone substrates (Castaño et al., 2016). Thus, previous studies have largely focused on the role of SETD7 on non-histone proteins, such as p53 (Chuikov et al., 2004), TAF10 (Kouskouti et al., 2004), DNMT1 (Estève et al., 2009), ER α (Subramanian et al., 2008), E2F1 (Kontaki and Talianidis, 2010), SOX2 (Fang et al., 2014), YAP (Oudhoff et al., 2013), LIN28A (Kim et al., 2014), and HIF1-alpha (Kim et al., 2016). Only a handful of studies showed SETD7 can bind on the promoter regions and regulate individual gene expression (Chen et al., 2012; Kofent et al., 2016). Although these data suggest SETD7 is directly involved in gene transcription, the question of whether SETD7-mediated H3K4me1 is essential for the transcriptional regulation of its target gene remains controversial.

Dynamic changes in SETD7 expression during developmental processes have been described, in particular during cardiac differentiation (Xie et al., 2013; Gifford et al., 2013). Recent studies have demonstrated that SETD7 is required for normal morphogenesis of zebrafish heart (Kim et al., 2015) and interacts with cardiac transcription factor Tbx1 in early cardiac development (Chen et al., 2012). While these findings suggest SETD7 plays a role in cardiac development, specific mechanisms by which SETD7 regulates CM differentiation have not been thoroughly investigated.

Here we show that SETD7 is a critical factor of cardiac differentiation. We found SETD7 expression was significantly upregulated during cardiac differentiation and modulated transcription of key regulatory genes for lineage commitment. Chromatin immunoprecipitation sequencing (ChIP-seq) of SETD7 in each stage of cardiac differentiation identified previously unknown genome-wide binding patterns of SETD7, and it revealed distinct SETD7 target genes at each stage of differentiation. In addition, our results identified stage-specific co-factors of SETD7, which are required for transcriptional regulation of the target genes. Cross-analysis with epigenetic dynamics elucidated unidentified interactions between SETD7 and H3K36me in cardiac differentiation. Finally, the loss of SETD7 resulted in irregular contractile activity of terminally differentiated CMs.

RESULTS

SETD7 Is Induced during Human Cardiac Differentiation

To study the role of epigenetic modifying enzymes in cardiac differentiation, we employed direct differentiation of human ESCs

(hESCs) to CMs as a model system of human cardiac development. Monolayers of CMs were successfully generated using a chemically defined protocol as previously described (Wu et al., 2015). Beating CMs exhibited normal Ca²⁺-handling properties and organized sarcomeric structures (Figures S1A–S1C). The expression of cardiac-specific genes appeared on day 5 of differentiation and reached maximal expression level on day 9 (Figure S1D). Based on the observed expression patterns and on previous studies (Paige et al., 2012), we selected four stages of differentiation that correspond to particular cell types: undifferentiated hESCs (differentiation day 0), mesodermal cells (MESs, differentiation day 2), cardiac progenitor cells (CPs, differentiation day 5), and beating CMs (differentiation day 9).

To identify the expression pattern of epigenetic modifying enzymes during cardiac differentiation, we performed RNA sequencing (RNA-seq) at each stage of CM differentiation. Cross-analysis with RNA-seq data of murine CM differentiation showed that SETD7 was significantly upregulated during CM differentiation in both human and mouse (Figure 1A). Analysis of the Expression Atlas Database revealed SETD7 was highly expressed in adult human and olive baboon (*Papio anubis*) heart tissue (Figure 1A). To confirm the expression of SETD7 in CMs, we generated CMs from hESCs and measured the expression of SETD7 during CM differentiation. qPCR of hESC-CMs showed a significant expression of SETD7 and TNNT2 (Figures 1B–1D). Immunoblotting (IB) analysis demonstrated an increased expression of SETD7 during cardiac differentiation (Figure 1E). Immunocytochemistry (ICC) with SETD7 and TNNT2 antibodies revealed that the majority of TNNT2⁺ cells exhibited nuclear localization of SETD7 (Figure 1F).

Dynamic Occupancy of SETD7 on Stage-Specific Target Genes of Cardiac Differentiation

To investigate the role of SETD7 in cardiac development, we performed ChIP-seq for SETD7 during the four stages of CM differentiation. Unsupervised K-means clustering identified five groups with distinct SETD7 enrichment patterns (Figure 1G; Table S1). Cluster 1 and cluster 3 sequentially lost SETD7 enrichment during CM differentiation, while cluster 2 retained SETD7 enrichment in hESC and mesoderm stages with reduced enrichment thereafter (Figure 1G). Cluster 4 transiently gained SETD7 enrichment but that was attenuated after the mesoderm stage; cluster 5 exhibited a sequential increase in SETD7 expression (Figure 1G). Average profiles of SETD7 enrichment on these target genes showed unique binding patterns of SETD7 on

Figure 1. Dynamic Target Genes of SETD7 during hESC-CM Differentiation

- (A) RNA-seq expression level of histone methyltransferases at each stage of CM differentiation in hESCs (human), mESCs (mouse), and heart tissues of human and olive baboon (*Papio anubis*). Heart tissue RNA-seq data were acquired from the Expression Atlas database.
- (B) Flow cytometry analysis of TNNT2⁺ cells in H7 hESCs and hESC-CMs (mean \pm SEM; n = 5).
- (C and D) qRT-PCR of TNNT2 (C) and SETD7 (D) in hESCs and hESC-CMs (*p < 0.05 and **p < 0.01, one-way ANOVA; mean \pm SEM; n = 4).
- (E) Immunoblot analysis of cell lysates at the indicated differentiation stages.
- (F) Immunostaining of TNNT2 and SETD7 in CMs (left). Cell counting of SETD7⁺ and/or TNNT2⁺ cells from immunostained images is shown (right). Scale bar, 10 μ m.
- (G) K-means clustering of SETD7 enrichment during CM differentiation. The y axis indicates log-transformed fold changes based on day 0 enrichment (top) or log-transformed fold changes based on RNA expression at day 0 (bottom).
- (H and I) Genome browser screenshots of ChIP-seq and RNA-seq for ACTC1 (H) and EOMES (I).
- (J) GO analysis of cluster 4 and cluster 5. Color code indicates negative log-transformed multiple testing adjusted p value.
- (K and L) Gene concept network displaying the gene names associated with the top signaling pathways identified in cluster 4 (K) and cluster 5 (L). See also Figure S1 and Table S1.

promoter and gene body regions (Figures 1H, 1I, and S1E–S1H). RNA expression of each cluster correlated with SETD7 enrichment, suggesting SETD7 deposition is associated with active gene transcription with unique functions at each stage of the CM differentiation (Figures 1G–1I).

Gene ontology (GO) enrichment analyses of SETD7 target genes showed important cardiac development pathways were upregulated at each stage of differentiation (Figure 1J). For example, genes in cluster 4 were enriched for embryo development pathways, including pattern specification process, somite and mesoderm development, and NOTCH and WNT-signaling pathways (Figures 1J, S1I, and S1J). In contrast, genes in cluster 5 were enriched for mature development pathways, such as heart morphogenesis, cardiac development, and cardiac muscle cell differentiation. A similar contrast between cluster 4 and cluster 5 genes was elucidated by gene concept network analysis in which a number of genes related to cardiac development predominated in cluster 5 while mesoderm-specific genes predominated in cluster 4 (Figures 1K and 1L). Interestingly, GO enrichment analyses of cluster 1 and cluster 3 also showed genes enriched for the regulation of stem cells, such as transcriptional regulation of pluripotent stem cells and expression of proliferation-enhancing genes POU5F1 (OCT4), SOX2, and NANOG (Figure S1J). Though SETD7 expression continuously increased during differentiation, SETD7 occupancy and expression of these target genes were significantly decreased. These data suggest SETD7 in the hESC stage is a transcriptional activator of these genes but may negatively affect the early stages of CM differentiation. Together, our ChIP-seq and RNA-seq data suggest there exist distinguishable functions for SETD7 at each stage of cardiac differentiation via stage-specific binding on its target genes.

Depletion of SETD7 Expression Results in Impaired Cardiac Differentiation

To understand the specific mechanisms by which SETD7 regulates CM differentiation, we used a transcription activator-like effector nuclease (TALEN)-mediated gene knockout system (Karakikes et al., 2017) to disrupt SETD7 expression in an HES3^{NKX2-5EGFP/w} hESC line that encodes EGFP under an NKX2-5 exon (Elliott et al., 2011). After screening clones transfected with a TALEN pair that targets start codon of SETD7, we successfully isolated heterozygous ($SETD7^{+/‐}$) and homozygous ($SETD7^{‐/‐}$) clones. The $SETD7^{‐/‐}$ clone showed a complete depletion of SETD7 expression in undifferentiated hESCs and on day 14 of CM differentiation (Figure 2A). In contrast to the $SETD7^{+/‐}$ clone, the $SETD7^{‐/‐}$ clone showed a significant decrease in NKX2-5-EGFP⁺ population, as well as a reduction of cardiac gene expression, such as MYH6 and TBX20, during CM differentiation (Figures 2B and 2C).

We confirmed these results in H7 hESCs stably expressing small hairpin RNA (shRNA) for SETD7, suggesting that SETD7 is necessary for CM differentiation (Figure 2D). We then generated an inducible shRNA system to study the effect of SETD7 specifically on CM differentiation. We introduced doxycycline (DOX)-inducible shRNA in H7 and HES3^{NKX2-5EGFP/w} lines, and we successfully generated stable clones carrying SETD7 and scramble shRNAs. In the presence of DOX, the expression of cardiac genes was significantly downregulated during CM differ-

entiation, which correlated with the suppression of NKX2-5-EGFP (Figures 2E–2G and S2A). No significant differences were detected in the scramble shRNA line. Interestingly, we did not detect any positive effects of SETD7 overexpression on the efficiency of CM differentiation, suggesting SETD7 alone was insufficient to facilitate CM differentiation (Figures S2B and S2C). Together, these results demonstrate SETD7 expression is necessary for CM differentiation.

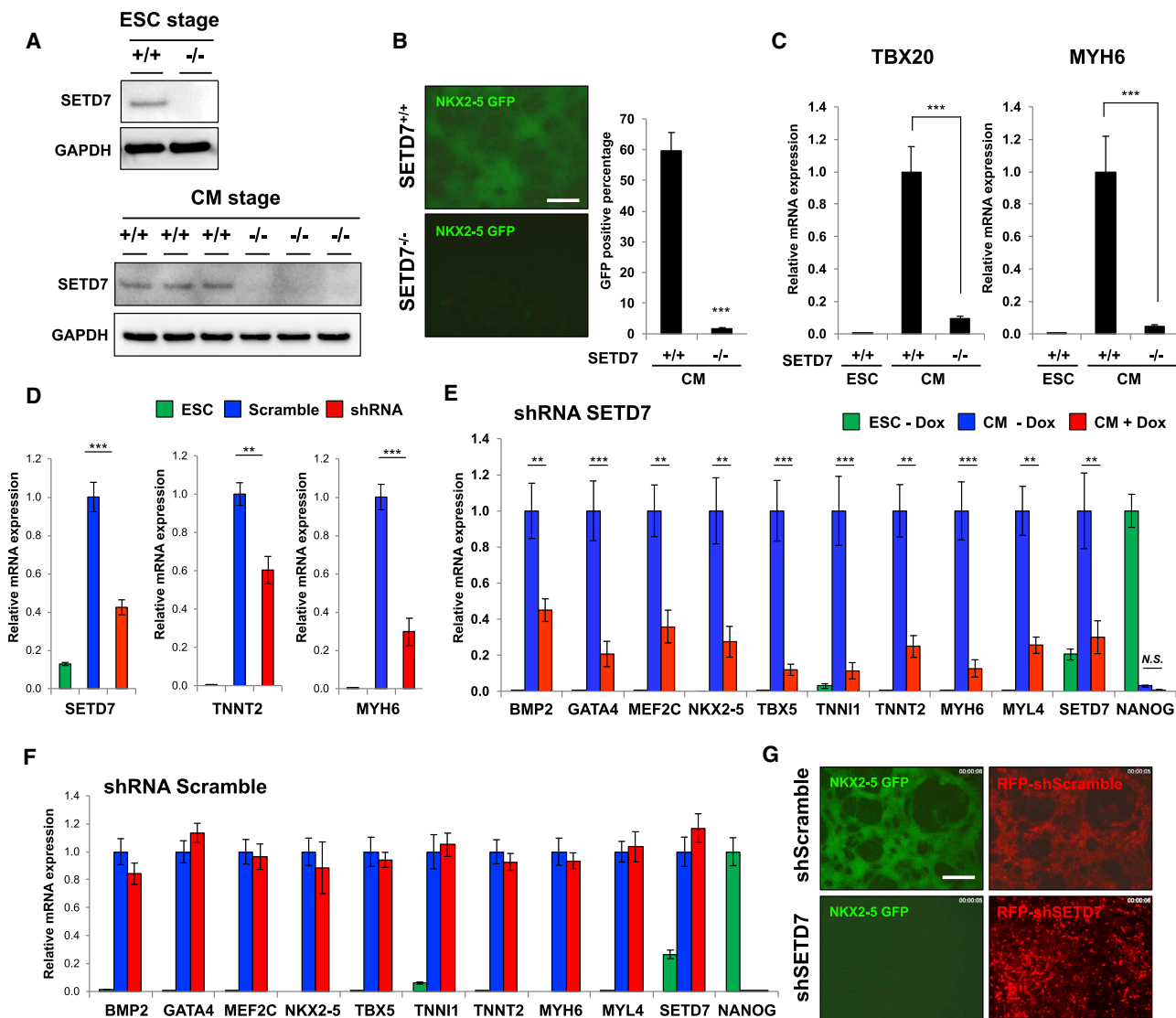
SETD7 Is Required for Mesoderm Lineage Commitment through Transcriptional Regulation of Key Regulatory Genes

ChIP-seq of SETD7 during CM differentiation revealed its dynamic target genes in each stage of differentiation. To examine how SETD7 regulates transcription of its target genes during the differentiation process, we first measured the effects of SETD7 knockout on the expression of mesoderm-specific genes. IB analysis confirmed upregulation of SETD7 expression during mesoderm specification in the $SETD7^{+/‐}$ line, whereas the $SETD7^{‐/‐}$ line showed a depletion of SETD7 expression (Figure 3A). Expression of key regulatory genes for early mesoderm lineage commitment (T, EVX1, DKK1, MIXL1, EOMES, and NODAL) and cardiac mesoderm lineage genes (GATA3 and MESP1) was significantly diminished in the $SETD7^{‐/‐}$ line (Figure 3B). GO analysis of RNA-seq at the mesoderm stage also showed downregulation of genes in the $SETD7^{‐/‐}$ line was associated with early cardiac differentiation pathways, such as ventricular cardiac muscle tissue development and ventricular cardiac muscle tissue morphogenesis (Figure S2D). In addition, rescue of SETD7 expression in the $SETD7^{‐/‐}$ line using a lentivirus-based overexpression system resulted in increased expression of mesoderm-specific genes (Figures 3C and 3D).

To confirm the indispensable role of SETD7 in mesodermal lineage commitment, we next generated embryoid bodies (EBs) that randomly differentiated into three germ layers (Figure S2E). EBs from the $SETD7^{‐/‐}$ line showed downregulation of endomesoderm-specific genes and upregulation of ectoderm-specific genes compared to the $SETD7^{+/‐}$ line (Figures 3E and 3F). Downregulation of endomesoderm genes was also observed in DOX-treated EBs carrying a Tet-inducible shRNA system for SETD7 (Figures S2F and S2G). Moreover, ChIP-seq analysis demonstrated SETD7 enriched on key regulatory genes for mesoderm specification in the mesoderm stage of CM differentiation (cluster 4). These data show SETD7 plays a key role in early cardiac differentiation through transcriptional regulation of mesoderm-specific genes.

SETD7 Is Necessary for Cardiac Lineage Specification

Next, we investigated the effects of SETD7 on cardiac lineage specification after the mesoderm stage. We suppressed SETD7 expression at different time points using a Tet-inducible shRNA system (Figure S2H). Consistent with our previous observations, differentiation efficiency was severely impaired when SETD7 suppression was initiated at day 0 of CM differentiation (Figures 2E, 3G, and 3H). Knockdown (KD) of SETD7 at day 3 and day 5 (early cardiac specification) also impaired differentiation efficiency compared to the scramble shRNA line or control treatment group (Figure 3G). In addition, downregulation

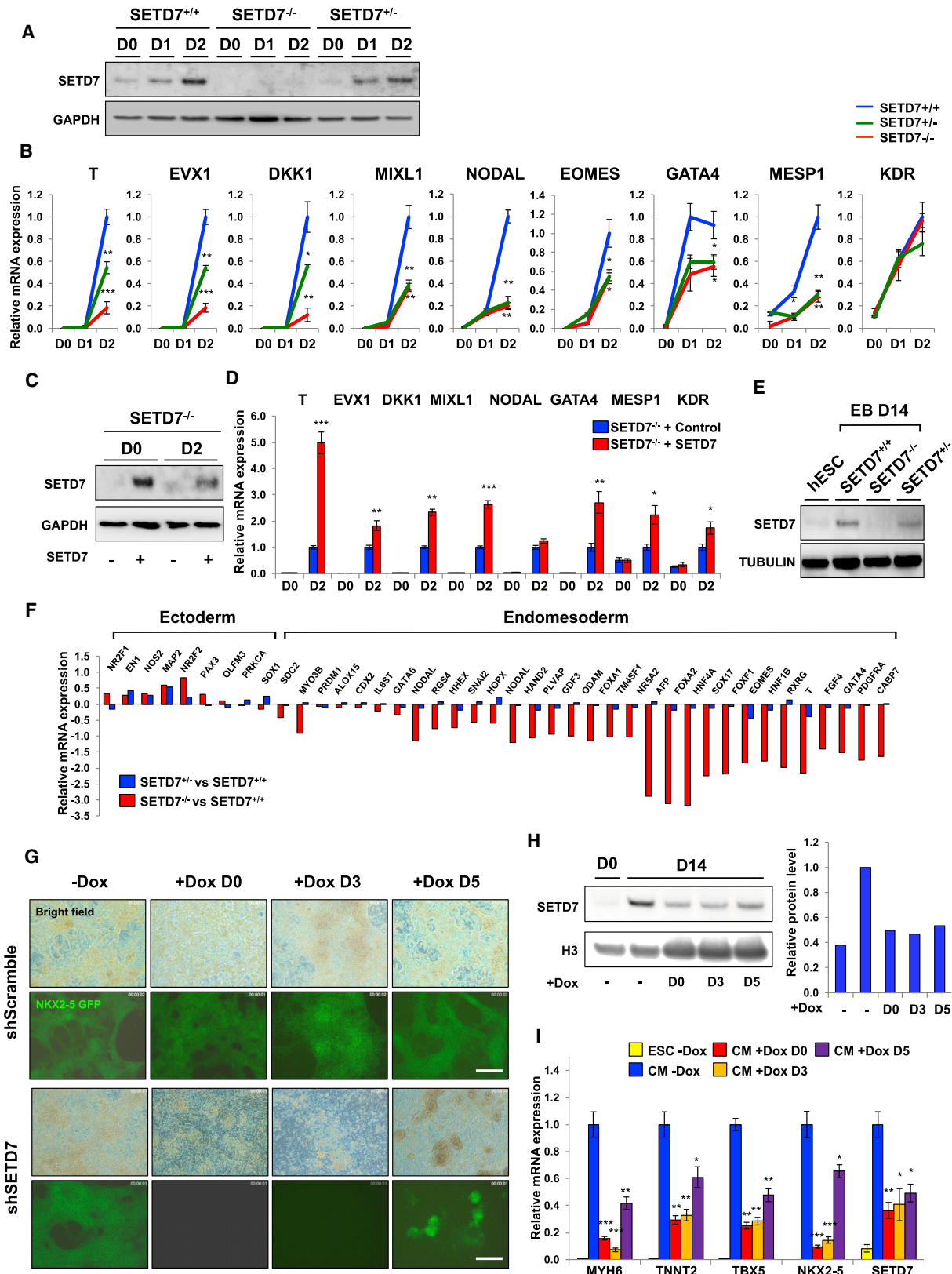
**Figure 2. SETD7 Is Necessary for CM Differentiation**

(A) Immunoblot analysis of cell lysates from HES3^{NKX2-5EGFP/w} hESC clone transfected with TALEN targeting start codon of SETD7 gene (top). Immunoblot analysis of cell lysate from *SETD7*^{+/+} and *SETD7*^{-/-} HES3^{NKX2-5EGFP/w}-derived CMs is shown (bottom) ($n = 3$). (B) NKX2-5-GFP expression in *SETD7*^{+/+} and *SETD7*^{-/-} HES3^{NKX2-5EGFP/w}-derived CMs (left). Flow cytometry of GFP⁺ cells is shown (right). Scale bar, 100 μ m. (C) qRT-PCR of TBX20 and MYH6 in *SETD7*^{+/+} and *SETD7*^{-/-} HES3^{NKX2-5EGFP/w}-derived CMs. (D) mRNA levels of SETD7, TNNT2, and MYH6 in control and SETD7 shRNA hESC-CMs. hESCs were infected with lentivirus carrying scramble or SETD7 shRNA. (E and F) Expression level of cardiac-related genes in hESCs and hESC-CMs expressing doxycycline-inducible scramble (F) or SETD7 shRNA (E). (G) Representative fluorescence microscopy images of hESC HES3^{NKX2-5EGFP/w}-derived CMs. Scale bar, 100 μ m. Statistical significance was obtained by one-way ANOVA; * $p < 0.05$, ** $p < 0.01$, and *** $p < 0.005$ (mean \pm SEM; $n = 4$). See also Figure S2.

of cardiac-specific genes was observed in the condition of SETD7 suppression at day 3 and day 5 (Figure 3*I*). In particular, major cardiac transcription factors (TFs), such as NKX2-5, TBX5, and GATA4, identified as target genes of SETD7 (cluster 5), were significantly downregulated in SETD7 KD (Figure 3*I*). The expression of cardiac-specific genes, such as MYH6 and TNNT2, was similarly attenuated with SETD7 KD (Figure 3*I*). These data suggest SETD7 expression in cardiac commitment is required for transcriptional activation of cardiac-specific genes.

Effects of SETD7 on Lineage-Specific Gene Expression of Non-CM Cell Types

As the IB analysis of SETD7 in human fetal tissues showed a high expression level of SETD7 in various tissue types, we tested whether SETD7 affects lineage differentiation processes of cell types other than CMs (Figures S2*I* and S2*J*). First, we differentiated *SETD7*^{+/+} and *SETD7*^{-/-} hESC lines to neuron precursor cells (NPCs, ectoderm) and hepatocyte-like cells (endoderm). Using currently available protocols (Song et al., 2009), we generated NPCs and hepatocyte-like cells expressing stage-specific



(legend on next page)

markers from both the *SETD7*^{-/-} and *SETD7*^{+/+} lines (Figures S3A–S3G). Interestingly, we observed an abnormal expression pattern of cell-type-specific genes, such as PAX6 (early NPC marker), NEUROG1 (late NPC marker), SOX17 (early endoderm lineage), NHE-4 (hepatocyte precursor), AFP (hepatocyte), and ALB (hepatocyte) (Figures S3C and S3F). Moreover, we observed *SETD7* is highly upregulated during both the NPC and hepatocyte-like cell differentiation processes (Figures S3A and S3E). These data suggest *SETD7* possesses unidentified roles in transcriptional regulation of certain lineage-specific genes during endodermal and ectodermal commitment.

We also tested whether depletion of *SETD7* affects differentiation of endothelial cells (ECs), a cell type that shares an early lineage path with CMs at the mesodermal and cardiac progenitor cell stages (Figures S3H–S3P). Using the monolayer-based, EB-free differentiation protocol previously described (Gu et al., 2017), we differentiated *SETD7*^{+/+} and *SETD7*^{-/-} hESC lines to ECs, which displayed cobblestone-like morphology representative of bona fide ECs (Figure S3H). The number of ECs obtained from the differentiation was also not altered, suggesting *SETD7* deficiency does not adversely affect the generation of bona fide ECs from hESCs (Figure S3I). However, mRNA expression levels of several endothelial functional genes were attenuated in the absence of *SETD7*. Endothelial markers CDH5, PECAM1, and VWF were significantly downregulated in *SETD7*^{-/-} hESC-ECs (Figures S3J–S3L). NOS3 expression was similarly downregulated, indicating *SETD7*^{-/-} hESC-ECs could not generate endothelial nitric oxide, a hallmark phenotype of endothelial dysfunction (Figure S3M). The expression level of the Endocan (ESM1) gene was also significantly reduced, indicating *SETD7*^{-/-} hESC-ECs were less angiogenic than wild-type (WT) (Figure S3N). Expression levels of cell surface adhesion molecules E-Selectin (SELE) and VCAM1 were not altered in the absence of inflammatory cytokines (Figures S3O and S3P). These data suggest *SETD7* is required in hESC-EC differentiation for normal expression of genes critical for EC function and homeostasis.

SETD7 Associates with Stage-Specific Co-factors for Transcriptional Regulation of Their Target Genes during Cardiac Differentiation

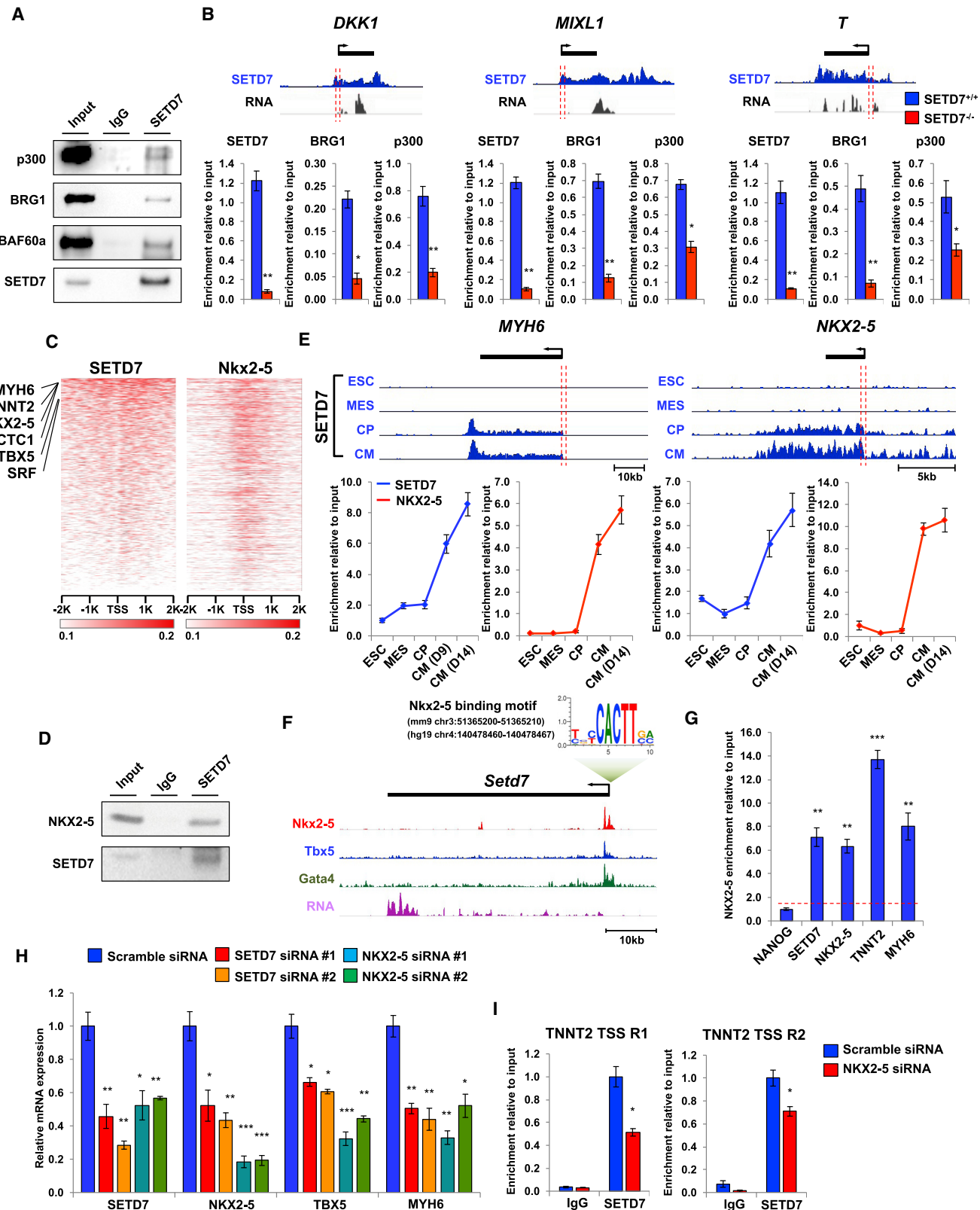
Next, we investigated the underlying mechanisms of *SETD7* on transcriptional regulation of its target genes during CM differentiation.

Previous studies have shown *SETD7* binds to BAF60a (mouse heart tissue) and BRG1 (ECs), factors known to be essential components of the SWI/SNF chromatin-remodeling complex (Chen et al., 2012; Okabe et al., 2012). Furthermore, *SETD7* is reported to interact with p300/CBP-associated factor (PCAF), another known co-factor of the SWI/SNF chromatin-remodeling complex (Huang et al., 2003; Ogiwara et al., 2011). Based on these findings, we tested whether *SETD7* is also associated with these co-factors during cardiac mesoderm commitment. Immunoprecipitation (IP) assay showed the interaction of *SETD7* with p300, BRG1, and BAF60a in mesoderm-stage cells (Figure 4A). We also detected the co-occupancy of p300, BRG1, and *SETD7* on the promoter regions of DKK1, MIXL1, and T genes in the cells of mesoderm stage in the *SETD7*^{+/+} line (Figure 4B). Interestingly, binding of p300 and BRG1 on target genes was significantly reduced in the *SETD7*^{-/-} line, suggesting *SETD7* recruited these co-transcription factors to the promoter regions of target genes (Figure 4B). The interaction between *SETD7* and chromatin-remodeling factors was not detected at the CM stage, consistent with a recent study showing that BRG1 expression was significantly decreased after cardiac mesoderm specification (Figure S4A) (Alexander et al., 2015). These data suggest *SETD7* possesses different binding partners in CM stages.

ChIP-seq analysis showed *SETD7* is targeting well-known cardiac TFs of NKX2-5, TBX5, and GATA4 in CP and CM stages (cluster 5). Because these cardiac TFs bind together forming a complex that regulates transcription of cardiac-specific genes during CM differentiation (Luna-Zurita et al., 2016), we speculated that *SETD7* interacts with these cardiac TFs to regulate cardiac lineage specification. To test this hypothesis, we cross-analyzed *SETD7* enrichment data with ChIP-seq of Nkx2-5, Mef2a, Gata4, Tbx5, and Srf in mouse tissue (He et al., 2011). We found the majority of *SETD7* target genes were shared with cardiac TFs, indicating a close association of *SETD7* with the cardiac TF network (Figures 4C and S4B). IP analysis of *SETD7* in CMs showed the interaction of *SETD7* and NKX2-5 (Figure 4D). ChIP-qPCR identified co-occupancy of *SETD7* and NKX2-5 on MYH6 and NKX2-5 promoters in a stage-dependent manner, revealing a coordinated network between *SETD7* and NKX2-5 for transcriptional regulation of the target genes (Figure 4E). We also identified a conserved binding motif of NKX2-5 in the promoter region of *SETD7* (Figure 4F). ChIP-seq of Nkx2-5,

Figure 3. SETD7 Is Required for Transcriptional Regulation of Lineage-Specific Genes during CM Differentiation

- (A) Immunoblot analysis of cell lysates from days 0, 1, and 2 of CM differentiation of *SETD7*^{+/+}, *SETD7*^{-/-}, and *SETD7*^{-/-} hESC lines.
- (B) qRT-PCR of mesoderm-specific genes in mesoderm lineage cells derived from *SETD7*^{+/+}, *SETD7*^{-/-}, and *SETD7*^{-/-} hESC lines.
- (C) Immunoblot analysis of cell lysates from hESCs and mesoderm lineage cells of *SETD7*^{-/-} lines carrying control or *SETD7* overexpression plasmid. Stable cell lines were generated using lentiviral overexpression system.
- (D) qRT-PCR of mesoderm-specific genes in hESCs and mesoderm lineage cells of *SETD7*^{-/-} lines carrying control or *SETD7* overexpression plasmid.
- (E) Immunoblot analysis of EB lysate from *SETD7*^{+/+}, *SETD7*^{-/-}, and *SETD7*^{-/-} hESC lines. α -tubulin was used as a loading control.
- (F) qRT-PCR of endomesoderm- and ectoderm-related genes in EBs from *SETD7*^{+/+} and *SETD7*^{-/-} hESC lines compared with *SETD7*^{+/+}. Total mRNA was extracted from day 14 of EB formation.
- (G) Representative fluorescence microscopy images of EGFP signal of hESC HES3^{NKX2-5EGFP/w}-derived CMs (day 14). Doxycycline was added to cell media on days 0, 3, and 5 of hESC-CM differentiation. Scale bar, 100 μ m.
- (H) Immunoblot analysis of *SETD7* protein levels in hESC HES3^{NKX2-5EGFP/w}-derived CMs (day 14) doxycycline-inducible shRNA for *SETD7* or scramble (left). Doxycycline was added to cell media on days 0, 3, and 5 of hESC-CM differentiation. Relative signal intensity of *SETD7* is shown (right).
- (I) qRT-PCR of cardiac-specific genes and *SETD7* expression levels in hESC HES3^{NKX2-5EGFP/w}-derived CMs (day 14) doxycycline-inducible shRNA for *SETD7* or scramble. Statistical significance was obtained by one-way ANOVA; *p < 0.05, **p < 0.01, and ***p < 0.005 (mean \pm SEM; n = 3). See also Figures 2 and 3 and Table S2.



(legend on next page)

Tbx5, and Gata4 showed that Nkx2-5 binds to the promoter region of Setd7 in mouse CMs (Figure 4F). ChIP-qPCR with primers targeting the NKX2-5-binding region confirmed the occupancy of NKX2-5 in the promoter of human SETD7 (Figure 4G). KD of NKX2-5 in CMs resulted in the downregulation of SETD7 expression (Figure 4H). Consistent with these observations, the loss of SETD7 suppressed Nkx2-5 expression in CMs, suggesting a positive feedback loop between NKX2-5 and SETD7 (Figure 4H). TBX5 and MYH6 expression was attenuated with KD of NKX2-5 or SETD7. In addition, binding of SETD7 on the TNNT2 promoter region was significantly decreased by the KD of NKX2-5, confirming that SETD7 and NKX2-5 are required for their shared target gene expression (Figure 4I). Taken together, these results demonstrate SETD7 interacts with stage-specific co-factors during human and mouse cardiac differentiation for transcriptional regulation of the target genes.

Correlation of SETD7 Enrichment with Active Chromatin Modifications during CM Differentiation

We next tested whether enzymatic activity of SETD7 is necessary for CM differentiation, given the role of SETD7 as an H3K4me1 methyltransferase. As a potent inhibitor of SETD7, PFI-2 suppressed the enzymatic activity of SETD7 on mono-methylation of H3K4 (Barsyte-Lovejoy et al., 2014) (Figure S4A). Treatment of PFI-2 during the entire CM differentiation process showed no significant differences in a TNNT2⁺ cell population at day 14 of differentiation, whereas the depletion of SETD7 itself severely reduced the TNNT2⁺ cell population (Figures 5A and 5B). The expression of mesoderm-specific genes was not decreased by PFI-2 treatment during mesoderm specification (Figures 5C and 5D). Interestingly, the global level of H3K4me1 also was not altered by either PFI-2 treatment or depletion of SETD7 (Figures 5A and 5C). These data suggest enzymatic activity of SETD7 is not necessary for CM differentiation whereas an unidentified role of SETD7 in epigenetic regulation exists.

To investigate the relationship between SETD7 and the epigenetic dynamics of CM differentiation, we next performed ChIP-seq at each stage of CM differentiation using antibodies against H3K27ac, followed by cross-analyses with public ChIP-seq datasets for H3K4me3, H3K27me3, and H3K36me3 (Paige et al., 2012). Spearman correlation analysis showed SETD7 genomic binding sites are enriched for active histone

markers (H3K27ac, H3K4me3, and H3K36me3), but not for a repressive marker (H3K27me3) (Figures S5B and S5C). We further tested the dynamic transitions of histone markers in individual SETD7 target genes. The enrichment of active histone markers showed similar profiles with SETD7 enrichment, whereas the repressive histone marker had an opposite pattern of enrichment compared to SETD7 (Figure 5E). As expected, RNA expression profiles of target genes were highly similar to SETD7 and active histone marker enrichment (Figure 5E). ChIP-qPCR confirmed co-occupancy of both SETD7 and active histone marker H3K4me3 in the cardiac genes during CM differentiation (Figures S5D–S5F). However, SETD7 enrichment was not detected on non-cardiac genes, such as SLC3A2 and NANOG, which also showed higher H3K4me3 modifications (Figures S5D–S5F). These data indicate SETD7 enrichment is highly correlated with the transition of active histone markers of its target genes during CM differentiation.

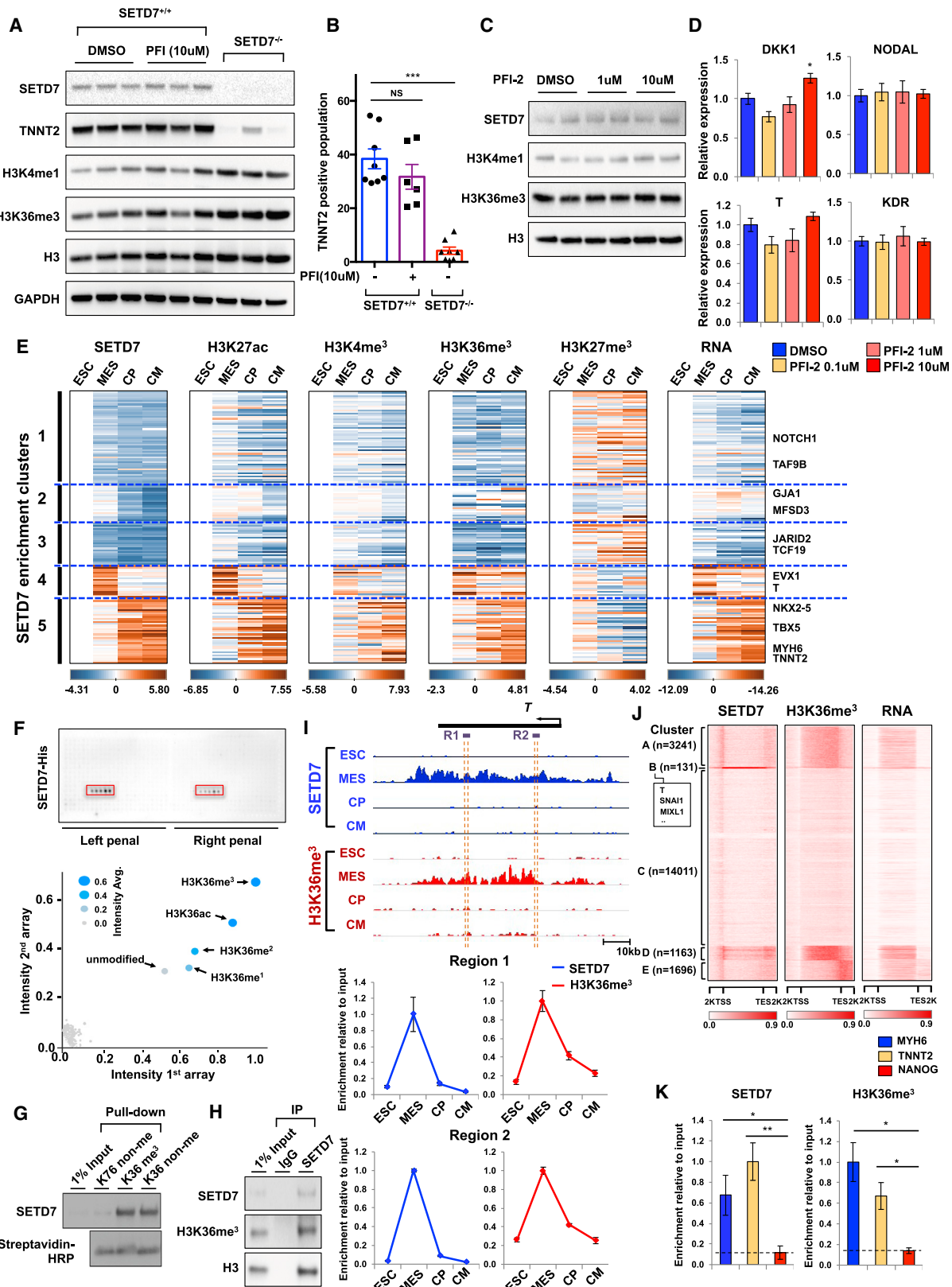
SETD7 Recognizes and Associates H3K36 Methylation on Gene Body Region of Its Target Genes during Cardiac Differentiation

We next determined which histone modifications are directly associated with SETD7. We performed a histone peptide array with active SETD7 protein purified from baculovirus-infected sf9 cells. SETD7 showed a strong affinity with H3K36me3, H3K36me2, H3K36me1, H3K36ac, and unmodified H3K36 (Figure 5F). Peptide array using active SETD7 tagged with glutathione S-transferase (GST) and FLAG confirmed binding of SETD7 on H3K36 peptides (Figure S5A). SETD7 was pulled down with H3K36-methylated peptide and non-methylated peptide, whereas no binding was detected with control peptide H3K79 (Figure 5G). Moreover, the interaction between SETD7 and H3K36me3 was confirmed by IP assay in CMs, indicating strong interactions between SETD7 and H3K36me3 in CMs (Figure 5H).

We further explored the correlation between H3K36 methylation and SETD7 enrichment on its target genes during CM differentiation. Consistent with the genome-wide enrichment pattern of H3K36me3, which was located on the gene body regions of actively transcribing genes (Bannister et al., 2005), ChIP-seq analysis of SETD7 showed broad occupancy of SETD7 on the gene body regions of target genes during CM

Figure 4. SETD7 Associates with Stage-Specific Co-factors for Active Gene Transcription of Its Target Genes

- (A) Immunoblot analysis of SETD7 immunoprecipitates (IP line) and cell lysates (input line) from mesoderm lineage cells derived from hESCs.
- (B) Genome browser screenshots of SETD7 ChIP-seq and RNA-seq profiles in DKK1, MIXL1, and T genes at the mesodermal stage of CM differentiation (top). ChIP-qPCR assay of SETD7, BRG1, and p300 at promoter regions of DKK1, MIXL1, and T genes during CM differentiation is shown (bottom). The sequence and genomic location of each primer are described in Table S2.
- (C) Relative enrichment levels of SETD7 (in human) and Nkx2-5 (in mouse) on transcription start site (TSS) of ortholog-coding genes in CMs. Heatmaps were ranked by SETD7 enrichment. ChIP-seq data were adapted from He et al. (2011).
- (D) Immunoblot analysis of SETD7 immunoprecipitates (IP line) and cell lysates (input line) from hESC-CMs.
- (E) Genome browser screenshots of SETD7 ChIP-seq profiles in MYH6 and NKX2-5 regions in four stages of CM differentiation (top). ChIP-qPCR of SETD7 and NKX2-5 enrichment at promoter regions of MYH6 and NKX2-5 genes during CM differentiation is shown (bottom). Orange bar indicates region targeted by qPCR.
- (F) Genome browser screenshot of Setd7 gene with a conserved NKX2-5 motif in the promoter region. Enrichment of Nkx2-5, Tbx5, and Gata4 on the promoter region of Setd7 promoter in mouse CMs is shown. ChIP-seq data were adapted from Luna-Zurita et al., 2016.
- (G) ChIP-qPCR of NKX2-5 enrichment at promoter regions of NANOG, SETD7, NKX2-5, TNNT2, and MYH6 in hESC-CMs.
- (H) qRT-PCR of mRNA expression of SETD7, NKX2-5, TBX5, and MYH6 genes in CMs transfected with two different sets of small interfering RNA (siRNA) for SETD7 and NKX2-5.
- (I) ChIP-qPCR of SETD7 and IgG at TSS regions of TNNT2 genes in NKX2-5 knockdown CMs. Statistical significance was obtained by one-way ANOVA; *p < 0.05, **p < 0.01, and ***p < 0.005 (mean ± SEM; n = 3). See also Figure S4.



(legend on next page)

differentiation (Figures S1E–S1H). Genome-wide correlation analysis also confirmed SETD7 enrichment was linked to H3K36me3 modification (Figure S6B). ChIP-qPCR with specific primers targeting gene body regions of T, MIXL1, NKX2-5, MYH6, and TNNT2 further demonstrated the co-occupancy of SETD7 and H3K36me3 in a stage-specific pattern (Figures 5I and S6C–S6F). Whole-genome analysis revealed increased transcription of genes with enrichment of both SETD7 and H3K36me3, suggesting co-occupancy of SETD7 and H3K36me3 can enhance transcription of their target genes (Figure 5J).

To test whether SETD7 is associated with H3K36me3 under physiological conditions, we next collected human left ventricular (LV) heart tissues from five healthy individuals, and we performed ChIP of SETD7 and H3K36me3. ChIP-qPCR showed co-occupancy of SETD7 and H3K36me3 in gene body regions of MYH6 and TNNT2, which was observed in human ESC-CMs (Figure 5K). We confirmed these data in two different fetal heart tissues (Figures S6G–S6I). Taken together, our findings demonstrate SETD7 is associated with H3K36me3 modifications on its target genes during CM differentiation.

SETD7 Is Not Necessary for Methylation of H3K36, but It Is Required for Pol II-Mediated Gene Transcription

We next tested whether SETD7 exerts its enzymatic activity on H3K36me3. *In vitro* methylation assay using active SETD7 protein showed SETD7 was not able to mediate H3K36me3 on H3K36 unmodified, H3K36me1, H3K36me2 peptide, and histone 3 protein (Figures 6A, 6B, and S7A). As expected, SETD7 mediated methylation of H3K4me1 on free histone 3 and octamer, but not on poly-nucleosome (Figure 6B). In addition, ChIP-seq and ChIP-qPCR analyses of H3K36me3 in the mesoderm stage of *SETD7^{+/+}* and *SETD7^{-/-}* lines revealed no significant decrease of H3K36me3 enrichment on its target genes (Figures 6C–6E and S7B). However, H3K36me3 level was suppressed by KD of SETD2, a major H3K36me3 methylase (Venkatesh et al., 2012) (Figures 6F and 6G). We found SETD7 enrichment on target genes was correlated with decreased H3K36me3 level by SETD2 KD (Figure 6G). These data indicate SETD7 is not necessary for H3K36me3, but bind-

ing of SETD7 on its target genes is highly dependent upon H3K36me3 status.

To further investigate the underlying mechanisms by which SETD7 controls the active function of H3K36me3 in transcriptional regulation of its target gene, we performed ChIP-seq with RNA polymerase II (Pol II)-S2P, Pol II in the *SETD7^{+/+}* and *SETD7^{-/-}* lines. The occupancy of Pol II-S2P on the gene body region of SETD7 target genes (cluster 4), especially near the transcription end site (TES), was markedly impaired by depletion of SETD7 (Figures 6H, 6I, and S7C). ChIP-qPCR with specific primers detecting the TESs of T and MIXL1 confirmed our findings (Figures 6J and 6K). On a genome-wide level, SETD7 also influenced the occupancy of Pol II-S2P and Pol II on the TES region (Figures 6H and S7C). We further analyzed the occupancy of Pol II-S2P of each cluster of SETD7 enrichment. Upon SETD7 depletion, we found decreased Pol II-S2P occupancy in the TES of genes, mostly with SETD7-H3K36me3 highly enriched clusters (cluster B and cluster D) (Figure S7E). Together, these data suggest SETD7 is necessary to recruit and facilitate Pol II-derived transcription of its target genes.

SETD7 Is Critical for Calcium-Handling Properties of Mature CMs

Given the high level of expression of SETD7 in hESC-CMs and in fetal and adult myocardial tissue (Figures 7A–7D), we next investigated the function of SETD7 in mature CMs (differentiation day 30–40). We generated highly pure CMs using a glucose starvation method (Sharma et al., 2015) and cultured them to day 30. We next introduced shRNA that targets SETD7 with a lentivirus system, and infected CMs were purified with puromycin to generate stable KD CMs. No cell death was observed in SETD7 KD CMs (Figure 7E). However, motion vector detection analysis (Hayakawa et al., 2014; Kopljari et al., 2017) showed increased SD of peak interval in SETD7 KD CMs compared to scramble CMs (Figure 7F). In addition, abnormal beating was observed in SETD7 KD CMs (Figures 7G and 7H).

In SETD7 KD CMs, no abnormal alignment of sarcomeric protein or mis-localization of connexin 43 was detected, a phenotype frequently observed in hypertrophic iPSC-CMs or in

Figure 5. SETD7 Is Linked with H3K36 Methylation on Its Target Genes

- (A) Immunoblot analysis of cell lysates from *SETD7^{+/+}* and *SETD7^{-/-}* lines at day 14 of CM differentiation. PFI-2 and DMSO were treated during the entire CM differentiation.
- (B) Flow cytometry of TNNT2⁺ cells of *SETD7^{+/+}* and *SETD7^{-/-}* at day 14 of CM differentiation. PFI-2 and DMSO were treated during the entire differentiation process (mean ± SEM; n = 8 for *SETD7^{+/+}* with DMSO and *SETD7^{-/-}*; n = 6 for *SETD7^{+/+}* with PFI-2).
- (C) Immunoblot analysis of mesodermal cells during CM differentiation. DMSO or PFI was treated for 2 days.
- (D) qRT-PCR of DKK1, NODAL, T, and KDR expression levels in mesodermal cells during CM differentiation. DMSO or PFI-2 was treated for 2 days.
- (E) Enrichment levels of histone markers and SETD7 at target genes in each of five clusters and of RNA expression.
- (F) Spot intensities of two peptide chip arrays. Each peptide chip contained 384 different histone modifications incubated with SETD7 protein. Blue dots represent mean signal intensities from two different peptide arrays.
- (G) Peptide pull-down assay of histone peptides with SETD7 protein. Biotinylated histone peptides were incubated with GST-SETD7 protein and pulled down with streptavidin-coated beads.
- (H) Immunoblot analysis of SETD7 immunoprecipitates (IP line) and cell lysates (input line) from hESC-CMs.
- (I) Genome browser screenshots of H3K36me3 and SETD7 ChIP-seq profiles in T at four stages of CM differentiation (top). ChIP-qPCR assay of H3K36me3 and SETD7 enrichment at the two gene body regions (dashed orange lines) of the T gene in four stages of CM differentiation is shown (bottom).
- (J) Genome-wide heatmaps of SETD7 and H3K36me3 enrichment in target gene bodies. RNA expression of target genes is shown in the rightmost heatmap. K-means clustering of SETD7 enrichment was used to sort heatmaps.
- (K) ChIP-qPCR for relative enrichment of SETD7 and H3K36me3 on gene body regions of MYH6, TNNT2, and NANOG genes in left ventricular tissue of healthy individuals (n = 5). Statistical significance was obtained by one-way ANOVA; *p < 0.05, **p < 0.01, and ***p < 0.005 (mean ± SEM; n = 3, B; n = 5, K). See also Figures S5 and S6.

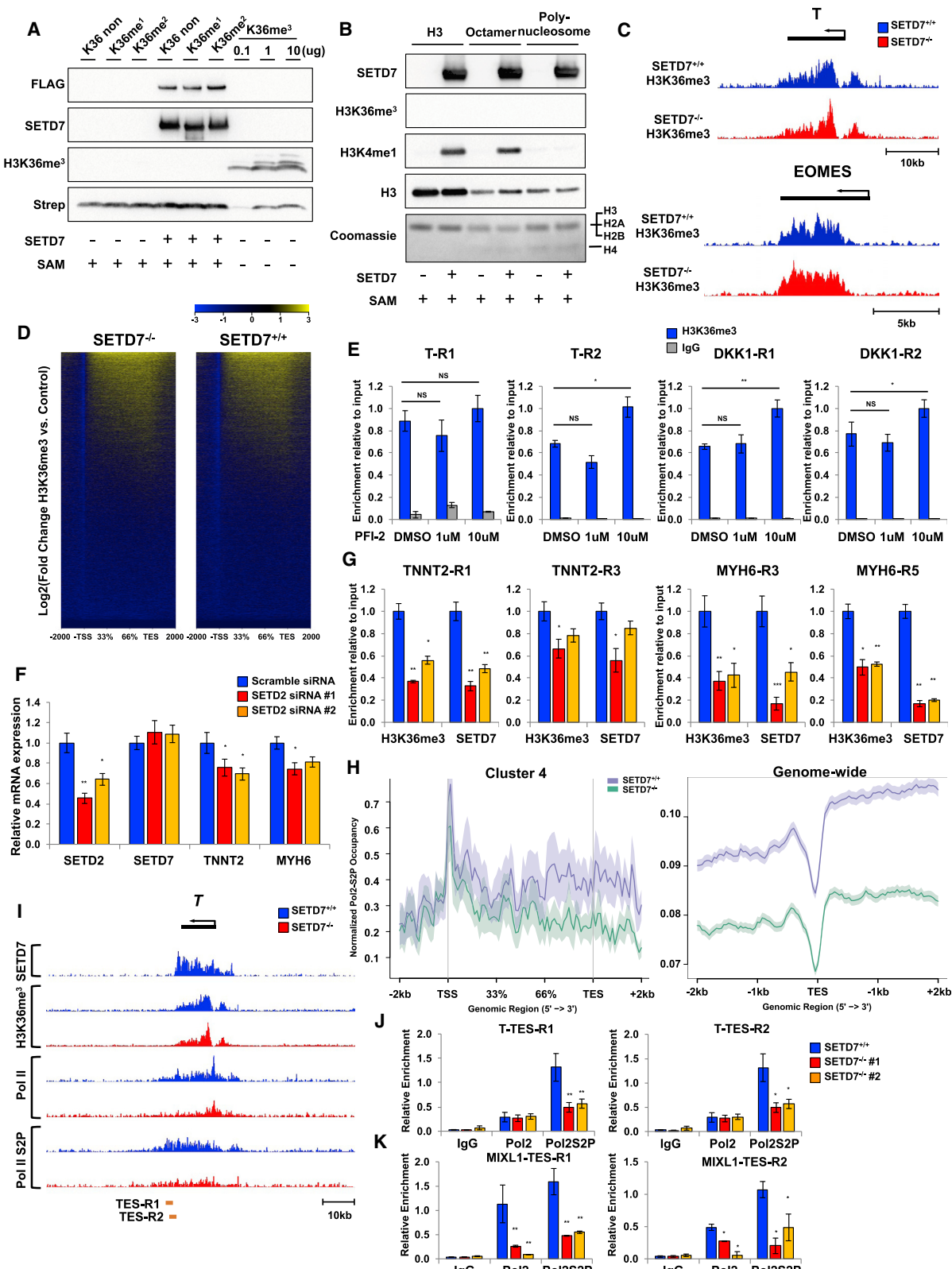


Figure 6. SETD7 Is Not Necessary for H3K36me3 but Is Required for Pol II-Mediated Gene Transcription

(A) Immunoblot analysis of SETD7 and H3K36me3. *In vitro* methylation assay was performed with histone peptides and active SETD7-FLAG protein. H3K36me3 peptide was used as a positive control.

(legend continued on next page)

damaged CMs (Figure 7I) (Burridge et al., 2016; Kostin et al., 2003). SETD7 KD did, however, result in irregular patterns of calcium transients, a major physiologic indicator of myocardial function (Figure 7J). While the diastolic calcium ratios were similar in scramble and SETD7 shRNA lines, the peak calcium ratios were significantly attenuated in the SETD7 shRNA group, indicating a decreased calcium amplitude (Figures 7K and 7L). The temporal parameters, such as decay tau, time to peak, and transient durations, were significantly elongated in SETD7 KD lines compared to the scramble line (Figures 7M–7O). Similarly, reduced calcium maximum rise rate (Figure 7P) and irregular calcium transients were observed in the SETD7 KD line (Figure 7Q). These data indicate SETD7 affects calcium handling of terminally differentiated CMs.

To explore the role of SETD7 in the modulation of calcium-handling properties, we measured the expression level of major calcium-handling genes in hESC-CMs. qRT-PCR showed the sarcoplasmic reticulum (SR) calcium-binding protein CASQ2 was significantly reduced in SETD7 KD CMs compared to control CMs (Figures 7R and 7S). CASQ2, by binding to the free calcium ion in the SR, regulates calcium load in the SR and contributes to regular calcium handling in CMs. The expression of ryanodine receptor 2 (RYR2), a major regulator of calcium release from the SR, was increased in SETD7 KD CMs (Figure 7T). Lower CASQ2 level in the SR downregulated the SR calcium storage capacity, while higher RYR2 expression level contributed to spontaneous calcium release events from the SR. Both the changes enhanced the probability of arrhythmia-like calcium-handling events, as we observed in SETD7 KD CMs. To confirm the direct transcriptional regulation of SETD7 on the CASQ2 gene, we further measured the direct binding of SETD7 to the CASQ2 genomic region using ChIP-qPCR. Our results showed a greater binding capacity of SETD7 on the gene body region of CASQ2 compared to that of IgG control, but lesser than the binding of SETD7 on MYH6 and TNNT2 (Figure 7U). These data suggest that SETD7 can partially interfere with CASQ2 expression in CMs. Taken together, our data show that SETD7 modulates calcium-handling properties of terminally differentiated CMs by regulating SR-related genes, such as CASQ2 and RYR2.

DISCUSSION

Our study identifies SETD7 as a key regulator of CM differentiation. ChIP-seq analysis of SETD7 at each stage of CM differentiation identified its stage-specific target genes and co-factors. We found SETD7 is essential for the transcriptional regulation

of key regulatory genes for cardiac lineage commitment, demonstrating the indispensable role of SETD7 in CM differentiation.

As co-factors in the SWI/SNF chromatin-remodeling complex, BAF60 and BRG1 are known to be crucial activators of cardiac regulatory genes during early cardiac development (Chen et al., 2012; Takeuchi et al., 2011). However, a recent study showed BRG1 possesses a dual role for cardiac mesoderm specification by repressing non-mesoderm genes through recruitment of the polycomb complex to target promoters (Alexander et al., 2015). These studies indicate the function of BRG1 in early cardiac development may differ by its co-factors. Our study showed SETD7 specifically interacts with BRG1 in the mesoderm stage and recruits it to the promoters of key regulatory genes for mesoderm lineage commitment.

Moreover, we show SETD7 partially shares its target genes with other cardiac TFs in the CM stages. We found a strong interaction between SETD7 and NKX2-5 and co-occupancy on the promoter region of target genes in CMs. A positive feedback loop between SETD7 and NKX2-5 was observed, indicating SETD7 serves as a critical component of major cardiac TF complexes and contributes to the transcriptional regulation of cardiac-specific genes during CM differentiation.

H3K36 methylation is known to play a critical role in gene transcription activation (Bannister et al., 2005), and it is considered a marker of gene transcription. H3K36 methylation is present in major cellular processes, such as gene silencing, DNA damage repair, and DNA replication, and its diverse function is dependent upon its binding protein (Brien et al., 2012; Musselman et al., 2012; Suzuki et al., 2016). Here we show SETD7 recognizes H3K36 methylation during the hESC-CM differentiation. Peptide array and IP assay demonstrate SETD7 has a high affinity with H3K36me3. The co-occupancy of SETD7 and H3K36me3 on the gene body region is highly correlated with gene activation during cardiac differentiation, suggesting SETD7 recognizes H3K36 methylation and regulates the transcription of target genes. We did not detect methylation activity of SETD7 on H3K36 residues, and KD or knockout of SETD7 showed no effect on H3K36me3 level of its target genes. These data suggest SETD7 recognizes H3K36 residue as a binding target, but not as a substrate for methylation.

At the transcriptional level, H3K36me3 is mainly mediated by SETD2 that conjugates with active Pol II during transcription elongation. This enrichment of H3K36me3 resulted in the suppression of cryptic transcription of target genes. However, KD of SETD2 remarkably reduced H3K36me3 levels of most of genes, whereas the effects of reduced H3K36me3 on gene transcription varied. In addition, H3K36me3 enrichment on the

(B) Immunoblot analysis of SETD7, H3K4me1, and H3K36me3. *In vitro* methylation assay was performed with histone H3, histone octamer, polynucleosome, and active SETD7-FLAG protein.

(C) Genome browser screenshots of H3K36me3 ChIP-seq profiles in T and EOMES genes at mesodermal stages of *SETD7^{+/+}* and *SETD7^{-/-}* lines.

(D) Genome-wide heatmaps of H3K36me3 enrichment on gene body region in *SETD7^{+/+}* and *SETD7^{-/-}*.

(E) ChIP-qPCR of H3K36 enrichment on gene body regions of T and DKK1 genes at mesoderm stage.

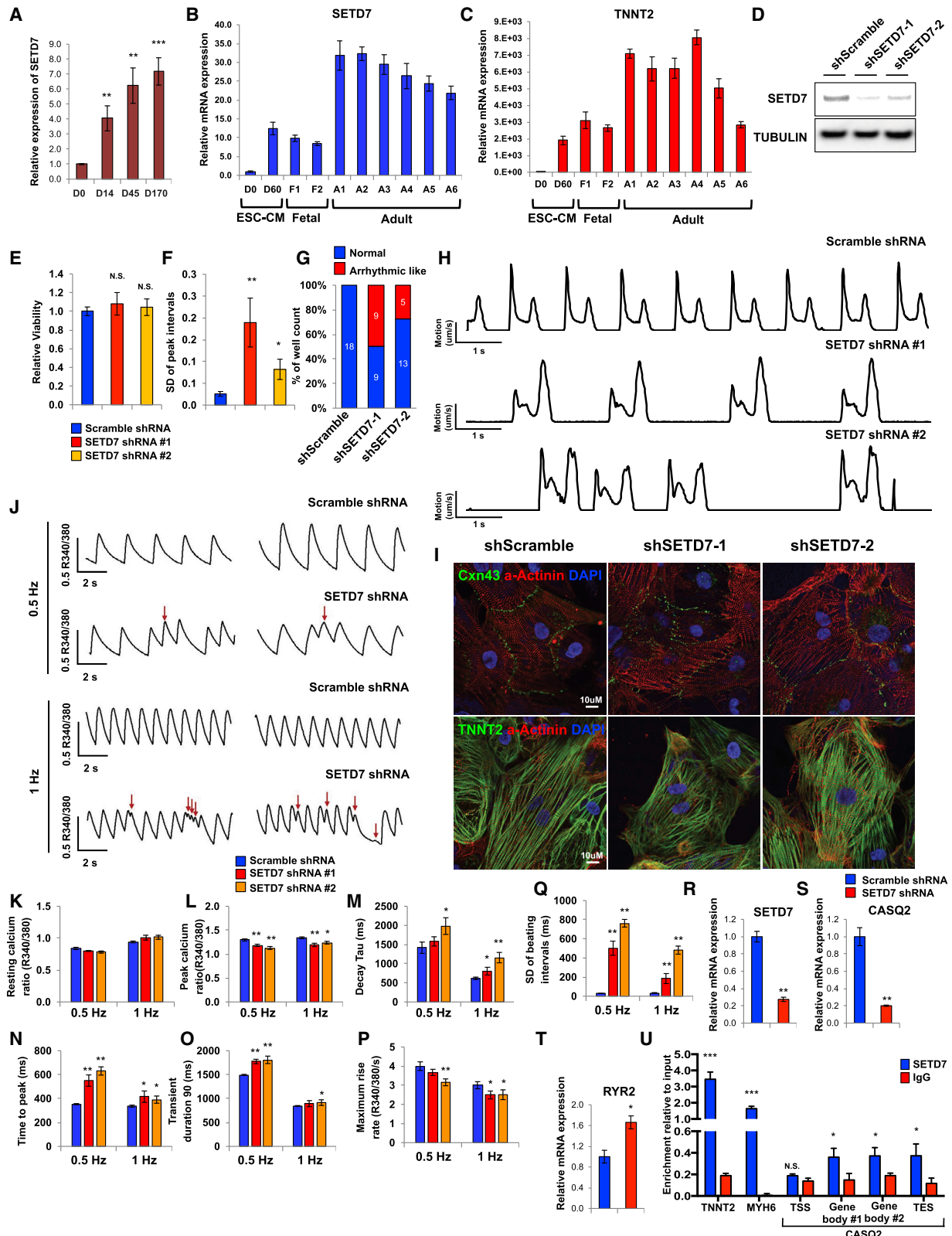
(F) qRT-PCR of SETD2, SETD7, TNNT2, and MYH6 expression levels in SETD2 knockdown CMs.

(G) ChIP-qPCR of SETD7 and H3K36 enrichment on gene body regions of TNNT2 and MYH6 genes in SETD2 knockdown CMs.

(H) Average profiles of Pol II-S2P enrichment in gene body regions of cluster 4 genes (left) and genome-wide level (right).

(I) Genome browser screenshots of SETD7, H3K36me3, Pol II, and Pol II-S2P ChIP-seq profiles on Brachyury (T) gene at mesoderm lineage of *SETD7^{+/+}* and *SETD7^{-/-}* lines.

(J and K) ChIP-qPCR of Pol II and Pol II-S2P enrichment at TES region of T (J) and DKK1 (K) genes in *SETD7^{+/+}* and *SETD7^{-/-}* lines at mesoderm stage. Statistical significance was obtained by one-way ANOVA; *p < 0.05 and **p < 0.01 (mean ± SEM; n = 3). See also Figure S7.

**Figure 7. SETD7 Is Critical for Calcium-Handling Properties of Mature CMs**

(A) SETD7 expression at various days of hESC-CM differentiation (n = 4).

(B and C) qRT-PCR of SETD7 (B) and TNNT2 (C) expression levels in hESC, hESC-CMs, fetal heart, and adult heart tissues.

(legend continued on next page)

endoderm-specific gene is necessary to transcription of its target gene during endoderm specification (Zhang et al., 2014). H3K36me3 may thus be involved not only in the suppression of cryptic transcription but also in the regulation of active gene transcription. In this study, we found the depletion of SETD7 exerted no significant effects on H3K36me3 level but instead reduced binding of Pol II-S2P on gene body and TES regions of SETD7 target genes. Taken together, SETD7 acts as a key regulator factor for active function of H3K36me3 in transcriptional regulation.

Given the critical role of SETD7 in CM differentiation, we next examined whether it modulates physiological function of terminally differentiated CMs *in vitro* and in adult human heart *in vivo*. Here, we found the loss of SETD7 resulted in abnormal calcium handling of CMs, driven by abnormal expression of CASQ2 and RYR2 expression. In the heart tissue of healthy donors, we confirmed SETD7 co-localizes with the H3K36me3 marker in the cardiac genes as we observed in hESC-CMs, suggesting SETD7 expression may be required for the maintenance of cardiac-specific genes in the adult heart.

In addition to the critical function of SETD7 in hESC-CM differentiation, our data indicate a role of SETD7 as a regulator of general transcriptional activation. We found SETD7 is highly expressed in other tissues and cell types such as hepatocyte-like cells and NPCs. Interestingly, SETD7 is continuously upregulated during the differentiation process of hepatocytes and NPCs, and it modulates the expression of lineage-specific genes in both cell types. Similarly, ablation of SETD7 disrupted the expression of endothelial genes in ESC-ECs, suggesting a role of SETD7 in endothelial function. Moreover, our ChIP-seq of SETD7 in the hESC stage showed genomic binding of SETD7 on broad gene body regions, despite its low expression in the hESC stage.

In conclusion, our study elucidates the multifaceted role of SETD7 in cardiac development, and it identifies SETD7 as a co-factor for H3K36me3 in transcriptional regulation of cardiac genes. We describe the role of epigenetic modifying enzyme in complex transcriptional regulatory mechanisms of cardiac gene expression, which can be utilized to develop therapeutic solutions for congenital heart disease and to improve methodologies for generating chamber-specific human pluripotent stem cell-derived CMs.

- (D) Immunoblot analysis of SETD7 in control and SETD7 knockdown lines.
- (E) Cell viability assay of control and SETD7 knockdown lines.
- (F) SD of peak intervals of control and SETD7 knockdown lines. Motion vector from movie images was recorded and analyzed with SONY Si8000 cell motion imaging system ($n = 18$).
- (G) Total number of wells with arrhythmic-beating hESC-CMs from control and SETD7 knockdown lines.
- (H) Representative traces of the motion velocity of hESC-CMs infected with scramble or SETD7 shRNA.
- (I) Immunostaining of CxN43, α -Actinin, and TNNT2 in control and SETD7 knockdown CMs.
- (J) Representative ratio-metric calcium-imaging traces of control and SETD7 knockdown CMs.
- (K) Resting calcium ratio.
- (L) Peak calcium ratio.
- (M) Decay Tau.
- (N) Time to peak.
- (O) Transient duration 90.
- (P) Maximum rise rate.
- (Q) SD of beating intervals of scramble and SETD7 shRNA lines ($n > 30$).
- (R-T) Relative RNA expression of SETD7 (R), CASQ2 (S), and RYR2 (T) in scramble and shRNA SETD7 groups.
- (U) ChIP-qPCR of SETD7 and IgG enrichment on TNNT2, MYH6, and CASQ2 genes in hESC-CMs ($n = 3$). Statistical significance was obtained by one-way ANOVA; * $p < 0.05$, ** $p < 0.01$, and *** $p < 0.005$ (mean \pm SEM).

STAR METHODS

Detailed methods are provided in the online version of this paper and include the following:

- KEY RESOURCES TABLE
- CONTACT FOR REAGENT AND RESOURCE SHARING
- EXPERIMENTAL MODEL AND SUBJECT DETAILS
 - Primary human samples
 - hESC lines and culture condition
 - Transcription activator-like effector nuclease (TALEN)-mediated gene knock-out ESC lines.
 - Lentivirus production and generation of stable cell line
- METHOD DETAILS
 - Differentiation of human PSCs to CMs
 - Immunoblotting and immunoprecipitation
 - RNA extraction and quantitative real-time polymerase chain reaction (qRT-PCR)
 - Chromatin immunoprecipitation and ChIP-seq
 - Intracellular calcium imaging
 - Immunofluorescence staining and confocal microscopy
- QUANTIFICATION AND STATISTICAL ANALYSIS
 - Chromatin immunoprecipitation and ChIP-seq analysis
 - RNA-seq analysis
- DATA AND SOFTWARE AVAILABILITY

SUPPLEMENTAL INFORMATION

Supplemental Information includes seven figures and three tables and can be found with this article online at <https://doi.org/10.1016/j.stem.2018.02.005>.

ACKNOWLEDGMENTS

We would like to thank Edouard G. Stanley for NFKX2-5EGFP/w hESC lines. We also thank Ates Akgun for generating hESC-CMs, Angelos Oikonomopoulos and Chun Liu for the protocol of hepatocyte differentiation, Soah Lee for CxN43 staining, and Sang-Ging Ong for helpful comments. This study was supported by the American Heart Association 17MERIT33610009 (J.C.W.) and 17IRG33410532 (I.K.); NIH R01 HL113006, R01 HL126527, R01 HL128170, R01 HL130020 (J.C.W.), and T32 EB009035 (D.T.P.); California Institute of Regenerative Medicine GC1R-06673-A (M.P.S.) and RT3-07798 (J.C.W.); and the National Research Foundation of Korea 2012R1A6A3A03039821 (J.L.).

AUTHOR CONTRIBUTIONS

Conceptualization, J.L. and J.C.W.; Methodology, V.T.; Formal Analysis, N.-Y.S., J.M.C., and Y.Z.; Investigation, J.L., M.-T.Z., H.G., Y.K., T.K., H.W., and D.T.P.; Data Curation, N.-Y.S., J.M.C., and Y.Z.; Writing – Original Draft, J.L.; Writing – Review & Editing, J.L., D.T.P., and K.D.W.; Resources, K.D.W. and I.K.; Supervision, M.P.S. and J.C.W.

DECLARATION OF INTERESTS

The authors declare no competing interests.

Received: May 19, 2017

Revised: December 15, 2017

Accepted: February 7, 2018

Published: March 1, 2018

REFERENCES

- Alexander, J.M., Hota, S.K., He, D., Thomas, S., Ho, L., Pennacchio, L.A., and Bruneau, B.G. (2015). Brg1 modulates enhancer activation in mesoderm lineage commitment. *Development* 142, 1418–1430.
- Bannister, A.J., Schneider, R., Myers, F.A., Thorne, A.W., Crane-Robinson, C., and Kouzarides, T. (2005). Spatial distribution of di- and tri-methyl lysine 36 of histone H3 at active genes. *J. Biol. Chem.* 280, 17732–17736.
- Barsyte-Lovejoy, D., Li, F., Oudhoff, M.J., Tatlock, J.H., Dong, A., Zeng, H., Wu, H., Freeman, S.A., Schapira, M., Senisterra, G.A., et al. (2014). (R)-PFI-2 is a potent and selective inhibitor of SETD7 methyltransferase activity in cells. *Proc. Natl. Acad. Sci. USA* 111, 12853–12858.
- Brien, G.L., Gambero, G., O'Connell, D.J., Jerman, E., Turner, S.A., Egan, C.M., Dunne, E.J., Jurgens, M.C., Wynne, K., Piao, L., et al. (2012). Polycomb PHF19 binds H3K36me3 and recruits PRC2 and demethylase NO66 to embryonic stem cell genes during differentiation. *Nat. Struct. Mol. Biol.* 19, 1273–1281.
- Burridge, P.W., Keller, G., Gold, J.D., and Wu, J.C. (2012). Production of de novo cardiomyocytes: human pluripotent stem cell differentiation and direct reprogramming. *Cell Stem Cell* 10, 16–28.
- Burridge, P.W., Sharma, A., and Wu, J.C. (2015). Genetic and epigenetic regulation of human cardiac reprogramming and differentiation in regenerative medicine. *Annu. Rev. Genet.* 49, 461–484.
- Burridge, P.W., Li, Y.F., Matsa, E., Wu, H., Ong, S.-G., Sharma, A., Holmström, A., Chang, A.C., Coronado, M.J., Ebert, A.D., et al. (2016). Human induced pluripotent stem cell-derived cardiomyocytes recapitulate the predilection of breast cancer patients to doxorubicin-induced cardiotoxicity. *Nat. Med.* 22, 547–556.
- Castaño, J., Morera, C., Sesé, B., Boue, S., Bonet-Costa, C., Martí, M., Roque, A., Jordan, A., and Barrero, M.J. (2016). SETD7 regulates the differentiation of human embryonic stem cells. *PLoS ONE* 11, e0149502.
- Chang, C.-P., and Bruneau, B.G. (2012). Epigenetics and cardiovascular development. *Annu. Rev. Physiol.* 74, 41–68.
- Chen, L., Fulcoli, F.G., Ferrentino, R., Martucciello, S., Illingworth, E.A., and Baldini, A. (2012). Transcriptional control in cardiac progenitors: Tbx1 interacts with the BAF chromatin remodeling complex and regulates Wnt5a. *PLoS Genet.* 8, e1002571.
- Chuikov, S., Kurash, J.K., Wilson, J.R., Xiao, B., Justin, N., Ivanov, G.S., McKinney, K., Tempst, P., Prives, C., Gamblin, S.J., et al. (2004). Regulation of p53 activity through lysine methylation. *Nature* 432, 353–360.
- Ding, Q., Lee, Y.-K., Schaefer, E.A.K., Peters, D.T., Veres, A., Kim, K., Kuperwasser, N., Motola, D.L., Meissner, T.B., Hendriks, W.T., et al. (2013). A TALEN genome-editing system for generating human stem cell-based disease models. *Cell Stem Cell* 12, 238–251.
- Ebert, A.D., Kodo, K., Liang, P., Wu, H., Huber, B.C., Riegler, J., Churko, J., Lee, J., de Almeida, P., Lan, F., et al. (2014). Characterization of the molecular mechanisms underlying increased ischemic damage in the aldehyde dehydrogenase 2 genetic polymorphism using a human induced pluripotent stem cell model system. *Sci. Transl. Med.* 6, 255ra130.
- Elliott, D.A., Braam, S.R., Koutsis, K., Ng, E.S., Jenny, R., Lagerqvist, E.L., Biben, C., Hatzistavrou, T., Hirst, C.E., Yu, Q.C., et al. (2011). NKX2-5(eGFP/w) hESCs for isolation of human cardiac progenitors and cardiomyocytes. *Nat. Methods* 8, 1037–1040.
- Estève, P.-O., Chin, H.G., Benner, J., Feehery, G.R., Samaranayake, M., Horwitz, G.A., Jacobsen, S.E., and Pradhan, S. (2009). Regulation of DNMT1 stability through SET7-mediated lysine methylation in mammalian cells. *Proc. Natl. Acad. Sci. USA* 106, 5076–5081.
- Fang, L., Zhang, L., Wei, W., Jin, X., Wang, P., Tong, Y., Li, J., Du, J.X., and Wong, J. (2014). A methylation-phosphorylation switch determines Sox2 stability and function in ESC maintenance or differentiation. *Mol. Cell* 55, 537–551.
- Gifford, C.A., Ziller, M.J., Gu, H., Trapnell, C., Donaghey, J., Tsankov, A., Shalek, A.K., Kelley, D.R., Shishkin, A.A., Issner, R., et al. (2013). Transcriptional and epigenetic dynamics during specification of human embryonic stem cells. *Cell* 153, 1149–1163.
- Gu, M., Shao, N.-Y., Sa, S., Li, D., Termglinchan, V., Ameen, M., Karakikes, I., Sosa, G., Grubert, F., Lee, J., et al. (2017). Patient-specific iPSC-derived endothelial cells uncover pathways that protect against pulmonary hypertension in BMPR2 mutation carriers. *Cell Stem Cell* 20, 490–504.e5.
- Hang, C.T., Yang, J., Han, P., Cheng, H.-L., Shang, C., Ashley, E., Zhou, B., and Chang, C.-P. (2010). Chromatin regulation by Brg1 underlies heart muscle development and disease. *Nature* 466, 62–67.
- Hayakawa, T., Kunihiro, T., Ando, T., Kobayashi, S., Matsui, E., Yada, H., Kanda, Y., Kurokawa, J., and Furukawa, T. (2014). Image-based evaluation of contraction-relaxation kinetics of human-induced pluripotent stem cell-derived cardiomyocytes: Correlation and complementarity with extracellular electrophysiology. *J. Mol. Cell. Cardiol.* 77, 178–191.
- He, A., Kong, S.W., Ma, Q., and Pu, W.T. (2011). Co-occupancy by multiple cardiac transcription factors identifies transcriptional enhancers active in heart. *Proc. Natl. Acad. Sci. USA* 108, 5632–5637.
- Huang, Z.-Q., Li, J., Sachs, L.M., Cole, P.A., and Wong, J. (2003). A role for cofactor-cofactor and cofactor-histone interactions in targeting p300, SWI/SNF and Mediator for transcription. *EMBO J.* 22, 2146–2155.
- Karakikes, I., Termglinchan, V., Cepeda, D.A., Lee, J., Diecke, S., Hendel, A., Itzhaki, I., Ameen, M., Shrestha, R., Wu, H., et al. (2017). A comprehensive TALEN-based knockout library for generating human-induced pluripotent stem cell-based models for cardiovascular diseases. *Circ. Res.* 120, 1561–1571.
- Kim, S.-K., Lee, H., Han, K., Kim, S.C., Choi, Y., Park, S.-W., Bak, G., Lee, Y., Choi, J.K., Kim, T.-K., et al. (2014). SET7/9 methylation of the pluripotency factor LIN28A is a nucleolar localization mechanism that blocks let-7 biogenesis in human ESCs. *Cell Stem Cell* 15, 735–749.
- Kim, J.-D., Kim, E., Koun, S., Ham, H.-J., Rhee, M., Kim, M.-J., and Huh, T.-L. (2015). Proper activity of histone H3 lysine 4 (H3K4) methyltransferase is required for morphogenesis during zebrafish cardiogenesis. *Mol. Cells* 38, 580–586.
- Kim, Y., Nam, H.J., Lee, J., Park, D.Y., Kim, C., Yu, Y.S., Kim, D., Park, S.W., Bhin, J., Hwang, D., et al. (2016). Methylation-dependent regulation of HIF-1 α stability restricts retinal and tumour angiogenesis. *Nat. Commun.* 7, 10347.
- Kofent, J., Zhang, J., and Spagnoli, F.M. (2016). The histone methyltransferase Setd7 promotes pancreatic progenitor identity. *Development* 143, 3573–3581.
- Kontaki, H., and Talianidis, I. (2010). Lysine methylation regulates E2F1-induced cell death. *Mol. Cell* 39, 152–160.
- Kopljari, I., De Bondt, A., Vinken, P., Teisman, A., Damiano, B., Goeminne, N., Van den Wyngaert, I., Gallacher, D.J., and Lu, H.R. (2017). Chronic drug-induced effects on contractile motion properties and cardiac biomarkers in human induced pluripotent stem cell-derived cardiomyocytes. *Br. J. Pharmacol.* 174, 3766–3779.
- Kostin, S., Rieger, M., Dammer, S., Hein, S., Richter, M., Klövekorn, W.-P., Bauer, E.P., and Schaper, J. (2003). Gap junction remodeling and altered connexin43 expression in the failing human heart. *Mol. Cell. Biochem.* 242, 135–144.

- Kouskouti, A., Scheer, E., Staub, A., Tora, L., and Talianidis, I. (2004). Gene-specific modulation of TAF10 function by SET9-mediated methylation. *Mol. Cell* 14, 175–182.
- Li, H., Zhong, Y., Wang, Z., Gao, J., Xu, J., Chu, W., Zhang, J., Fang, S., and Du, S.J. (2013). Smyd1b is required for skeletal and cardiac muscle function in zebrafish. *Mol. Biol. Cell* 24, 3511–3521.
- Luna-Zurita, L., Stirnimann, C.U., Glatt, S., Kaynak, B.L., Thomas, S., Baudin, F., Samee, M.A.H., He, D., Small, E.M., Mileikovsky, M., et al. (2016). Complex interdependence regulates heterotypic transcription factor distribution and coordinates cardiogenesis. *Cell* 164, 999–1014.
- Musselman, C.A., Avvakumov, N., Watanabe, R., Abraham, C.G., Lalonde, M.-E., Hong, Z., Allen, C., Roy, S., Nuñez, J.K., Nickoloff, J., et al. (2012). Molecular basis for H3K36me3 recognition by the Tudor domain of PHF1. *Nat. Struct. Mol. Biol.* 19, 1266–1272.
- Ng, S.B., Bigham, A.W., Buckingham, K.J., Hannibal, M.C., McMillin, M.J., Gildersleeve, H.I., Beck, A.E., Tabor, H.K., Cooper, G.M., Mefford, H.C., et al. (2010). Exome sequencing identifies MLL2 mutations as a cause of Kabuki syndrome. *Nat. Genet.* 42, 790–793.
- Nimura, K., Ura, K., Shiratori, H., Ikawa, M., Okabe, M., Schwartz, R.J., and Kaneda, Y. (2009). A histone H3 lysine 36 trimethyltransferase links Nkx2-5 to Wolf-Hirschhorn syndrome. *Nature* 460, 287–291.
- Ogiwara, H., Ui, A., Otsuka, A., Satoh, H., Yokomi, I., Nakajima, S., Yasui, A., Yokota, J., and Kohno, T. (2011). Histone acetylation by CBP and p300 at double-strand break sites facilitates SWI/SNF chromatin remodeling and the recruitment of non-homologous end joining factors. *Oncogene* 30, 2135–2146.
- Okabe, J., Orlowski, C., Balerczyk, A., Tikellis, C., Thomas, M.C., Cooper, M.E., and El-Osta, A. (2012). Distinguishing hyperglycemic changes by Set7 in vascular endothelial cells. *Circ. Res.* 110, 1067–1076.
- Oudhoff, M.J., Freeman, S.A., Couzens, A.L., Antignano, F., Kuznetsova, E., Min, P.H., Northrop, J.P., Lehnertz, B., Barsyte-Lovejoy, D., Vedadi, M., et al. (2013). Control of the hippo pathway by Set7-dependent methylation of Yap. *Dev. Cell* 26, 188–194.
- Paige, S.L., Thomas, S., Stoick-Cooper, C.L., Wang, H., Maves, L., Sandstrom, R., Pabon, L., Reinecke, H., Pratt, G., Keller, G., et al. (2012). A temporal chromatin signature in human embryonic stem cells identifies regulators of cardiac development. *Cell* 151, 221–232.
- Sharma, A., Li, G., Rajarajan, K., Hamaguchi, R., Burridge, P.W., and Wu, S.M. (2015). Derivation of highly purified cardiomyocytes from human induced pluripotent stem cells using small molecule-modulated differentiation and subsequent glucose starvation. *J. Vis. Exp.* (97), 52628.
- Shen, L., Shao, N., Liu, X., and Nestler, E. (2014). ngs.plot: Quick mining and visualization of next-generation sequencing data by integrating genomic databases. *BMC Genomics* 15, 284.
- Song, Z., Cai, J., Liu, Y., Zhao, D., Yong, J., Duo, S., Song, X., Guo, Y., Zhao, Y., Qin, H., et al. (2009). Efficient generation of hepatocyte-like cells from human induced pluripotent stem cells. *Cell Res.* 19, 1233–1242.
- Subramanian, K., Jia, D., Kapoor-Vazirani, P., Powell, D.R., Collins, R.E., Sharma, D., Peng, J., Cheng, X., and Vertino, P.M. (2008). Regulation of estrogen receptor α by the SET7 lysine methyltransferase. *Mol. Cell* 30, 336–347.
- Suzuki, S., Kato, H., Suzuki, Y., Chikashige, Y., Hiraoka, Y., Kimura, H., Nagao, K., Obuse, C., Takahata, S., and Murakami, Y. (2016). Histone H3K36 trimethylation is essential for multiple silencing mechanisms in fission yeast. *Nucleic Acids Res.* 44, 4147–4162.
- Takeuchi, J.K., Lou, X., Alexander, J.M., Sugizaki, H., Delgado-Olguín, P., Holloway, A.K., Mori, A.D., Wylie, J.N., Munson, C., Zhu, Y., et al. (2011). Chromatin remodelling complex dosage modulates transcription factor function in heart development. *Nat. Commun.* 2, 187.
- Vallaster, M., Vallaster, C.D., and Wu, S.M. (2012). Epigenetic mechanisms in cardiac development and disease. *Acta Biochim. Biophys. Sin. (Shanghai)* 44, 92–102.
- Venkatesh, S., Smolle, M., Li, H., Gogol, M.M., Saint, M., Kumar, S., Natarajan, K., and Workman, J.L. (2012). Set2 methylation of histone H3 lysine 36 suppresses histone exchange on transcribed genes. *Nature* 489, 452–455.
- Wamstad, J.A., Alexander, J.M., Truty, R.M., Shrikumar, A., Li, F., Eilertson, K.E., Ding, H., Wylie, J.N., Pico, A.R., Capra, J.A., et al. (2012). Dynamic and coordinated epigenetic regulation of developmental transitions in the cardiac lineage. *Cell* 151, 206–220.
- Wang, H., Cao, R., Xia, L., Erdjument-Bromage, H., Borchers, C., Tempst, P., and Zhang, Y. (2001). Purification and functional characterization of a histone H3-lysine 4-specific methyltransferase. *Mol. Cell* 8, 1207–1217.
- Wu, H., Lee, J., Vincent, L.G., Wang, Q., Gu, M., Lan, F., Churko, J.M., Sallam, K.I., Matsa, E., Sharma, A., et al. (2015). Epigenetic regulation of phosphodiesterases 2A and 3A underlies compromised β -adrenergic signaling in an iPSC model of dilated cardiomyopathy. *Cell Stem Cell* 17, 89–100.
- Xie, W., Schultz, M.D., Lister, R., Hou, Z., Rajagopal, N., Ray, P., Whitaker, J.W., Tian, S., Hawkins, R.D., Leung, D., et al. (2013). Epigenomic analysis of multilineage differentiation of human embryonic stem cells. *Cell* 153, 1134–1148.
- Zhang, Y., Xie, S., Zhou, Y., Xie, Y., Liu, P., Sun, M., Xiao, H., Jin, Y., Sun, X., Chen, Z., et al. (2014). H3K36 histone methyltransferase Setd2 is required for murine embryonic stem cell differentiation toward endoderm. *Cell Rep.* 8, 1989–2002.

STAR★METHODS**KEY RESOURCES TABLE**

REAGENT or RESOURCE	SOURCE	IDENTIFIER
Antibodies		
Anti-SETD7	Abcam	ab124708 RRID:AB_10975432
Anti-SETD7	Abcam	ab14820 RRID:AB_301497
Anti-SETD7	Thermo Fisher	730055 RRID:AB_2532856
Anti-p300	Active Motif	61401 RRID:AB_2716754
Anti-p300	Abcam	ab54984 RRID:AB_944580
Anti-tubulin	Abcam	ab40742 RRID:AB_880625
Anti-GAPDH	Thermo Fisher	MA5-15738-HRP RRID:AB_2537659
Anti-H3K36me3	Active Motif	61101 RRID:AB_2615073
Anti-H3K36me3	Active Motif	61021 RRID:AB_2614986
Anti-H3K36me3	Abcam	ab9050 RRID:AB_306966
Anti-H3K27ac	Active Motif	39133 RRID:AB_2561016
Anti-H3K4me1	Active Motif	39635
Anti-H3	Abcam	ab53528 RRID:AB_880440
Anti-NKX2-5	Abcam	ab91196 RRID:AB_10562620
Anti-NKX2-5	R and D System	AF2444 RRID:AB_355269
Anti-BRG1	Abcam	ab110641 RRID:AB_10861578
Anti-BRG1	Abcam	ab196315
Anti-SMARCD1	Sigma-Aldrich	HPA004101 RRID:AB_1080026
Anti-Cardiac Troponin T Antibody (3D6)	Thermo Fisher	MA1-24616 RRID:AB_2206552
Anti-Pol II (8WG16)	BioLegend	664906 RRID:AB_2565554
Anti- RNA polymerase II CTD repeat YSPTSPS	Abcam	ab5095 RRID:AB_304749
Anti-Cardiac Troponin T	Abcam	ab45932 RRID:AB_956386
Anti-Sarcomeric Alpha Actinin	Abcam	ab68167 RRID:AB_11157538
Anti-Nestin (2C1.3A11)	Abcam	ab18102 RRID:AB_444246
Anti-PAX6	Abcam	ab5790 RRID:AB_305110
Anti-Alpha-1 fetoprotein	Dako	A0008 RRID:AB_2650473
Anti-Albumin	Bethyl Laboratories	A80-129A RRID:AB_67016
Anti-Connexin-43	Sigma-Aldrich	C6219 RRID:AB_476857
normal mouse IgG	Santa Cruz	sc-2025 RRID:AB_737182
normal rabbit IgG	Santa Cruz	sc-2027 RRID:AB_737197
Biological Samples		
Human heart tissues	Wu lab tissue bank	N/A
Chemicals, Peptides, and Recombinant Proteins		
Fetal bovine serum	Hyclone	SH30071.03
GlutaMax supplement	Thermo Fisher Scientific	35050061
PSC Neural Induction Medium	Thermo Fisher Scientific	#A1647801
Gelatin Solution	Sigma-Aldrich	G1393
Essential 8 medium	Thermo Fisher Scientific	A1517001
Matrigel matrix	Corning	354277
Accutase	Sigma-Aldrich	A6964
ROCK inhibitor	Tocris	Y-27632
Lipofectamine 2000	Thermo Fisher Scientific	11668019
SETD7 protein	Active Motif	31496
SETD7 protein (Active)	Abcam	ab167960

(Continued on next page)

Continued

REAGENT or RESOURCE	SOURCE	IDENTIFIER
Histone H3 (44 - 63) - GGK(Biotin), biotin - labeled	Anaspec	AS-64642-1
Histone H3 (69 - 89) - K(Biotin)	Anaspec	AS-65297-1
Histone H3 (1 - 21), Biotinylated	Anaspec	AS-61702
Histone H3 (21 - 44) - GK(Biotin), biotin - labeled	Anaspec	AS-64440-025
[Lys(Me3)36] - Histone H3 (21 - 44) - GK(Biotin), H3K36(Me3), biotin - labeled	Anaspec	AS-64441-025
Recombinant Histone H3.3 (Human)	Active Motif	31295
Recombinant Polynucleosomes	Active Motif	31468
Dynabeads Protein A	Thermo Fisher Scientific	10001D
Dynabeads Protein G	Thermo Fisher Scientific	10003D
Critical Commercial Assays		
RNeasy Plus Mini Kit	QIAGEN	74136
MODified Histone Peptide Array	Active Motif	13001
Nextera DNA Sample Preparation Kit	Illumina	FC-121-1030
NEBNext Ultra II DNA Library Prep Kit for Illumina	NEB	E7645S
ChIP DNA Clean & concentrator	Zymo Research	D5205
Deposited Data		
Expression Atlas Database	Expression Atlas Data base	E-MTAB-30352
Expression Atlas Database	Expression Atlas Data base	E-MTAB-513
Expression Atlas Database	Expression Atlas Data base	E-MTAB-2836
Expression Atlas Database	Expression Atlas Data base	E-MTAB-2848
RNA-seq and ChIP-seq raw and processed data	This paper	GEO: GSE107785
ChIP-seq of mouse cardiac TFs	PMID: 21415370	GEO: GSE21529
ChIP-seq of mouse cardiac TFs	PMID: 26875865	GEO: GSE72223
ChIP-seq of histone marker (H3K4me3, H3K27me3, H3K36me3) (H7-CMs)	PMID: 22955617	GEO: GSE35583
Experimental Models: Cell Lines		
hESC H7	WiCell Research Institute	WA07
HES3NKX2-5eGFP/w human ESCs	Dr. Edouard G Stanley	N/A
hESC H7 SETD7 ^{-/-}	This paper	N/A
hESC H7 SETD7 ^{+/-}	This paper	N/A
Oligonucleotides		
See Table S2 for ChIP-qPCR primers	This paper	Table S2
Recombinant DNA		
pLKO control	Dharmacon	RHS6848
pLKO-shSETD7	Dharmacon	TRCN0000078632
		TRCN0000078628
		TRCN0000078630
pTRIPZ-shControl	Dharmacon	RHS4743
pTRIPZ-shSETD7	Dharmacon	V2THS_230143
		V2THS_99174
Software and Algorithms		
GraphPad Prism version 7.0	GraphPad Software	N/A
FlowJo v10	FLOWJO, LLC	N/A
ImageJ	NIH	N/A
SAMtools	Genome Research Limited	http://www.htslib.org/
HTSeq	EBML	http://www-huber.embl.de/HTSeq/doc/overview.html

(Continued on next page)

Continued

REAGENT or RESOURCE	SOURCE	IDENTIFIER
DESeq	Bioconductor	http://bioconductor.org/packages/release/bioc/html/DESeq.html
Bowtie	John Hopkins University	http://bowtie-bio.sourceforge.net/index.shtml
STAR	Cold Spring Harbor Laboratory	https://github.com/alexdobin/STAR
FastQC	Babraham Institute	http://www.bioinformatics.babraham.ac.uk/projects/fastqc/
PhantomPeak	Harvard	https://code.google.com/archive/p/phantompeakqualtools/
Bedtools	the University of Utah	http://bedtools.readthedocs.io/en/latest/
IGV genome browser	Broad Institute	https://www.broadinstitute.org/igv/
Ngs.plot	Ichan School of Medicine at Mount Sinai	https://github.com/shenlab-sinai/ngsplot
Cytoscape	NIH	http://www.cytoscape.org/
iRegulon	University of Leuven	http://iregulon.aertslab.org/

CONTACT FOR REAGENT AND RESOURCE SHARING

Further information and requests for resources and reagents should be directed to and will be fulfilled by the Lead Contact, Joseph Wu (joewu@stanford.edu).

EXPERIMENTAL MODEL AND SUBJECT DETAILS**Primary human samples**

The protocols used in this study were approved by the Institutional Review Board (IRB) at Stanford University. The written consent was obtained from all the patients involved in this study. For details on samples, see [Table S3](#).

hESC lines and culture condition

H7 hESC line was obtained from WiCell Research Institute (WA07). Dr. Edouard G Stanley kindly provided HES3^{NKX2-5eGFP/w} human ESC line. Human ESC lines (H7 and HES3) were maintained on Matrigel-coated plates (BD Biosciences) in Essential 8 Medium (GIBCO, Life Technology). The medium was changed every day.

Transcription activator-like effector nuclease (TALEN)-mediated gene knock-out ESC lines.

TALEN pair vectors were designed to target start codon of SETD7 and constructed using rapid TALEN assembly system as previously described ([Ding et al., 2013](#)). Both TALEN pair vectors were delivered into HES3^{NKX2-5eGFP/w} hESC line by nucleofection using P3 Primary Cell 4D-Nucleofector X Kit (Lonza). After 48 hr following nucleofection, transfected cells were enriched using fluorescence-activated cell sorting for double positive cells (GFP⁺/RFP⁺). Subsequently, sorted cells were expanded, manually picked and genotyped by direct sequencing of the PCR products and TOPO-cloned PCR products.

Lentivirus production and generation of stable cell line

The lentiviral shRNA plasmid sets—pLKO control, pLKO-shSETD7 (Clone ID: 030648.2-985s21c1), pTRIPZ shControl, pTRIPZ SETD7 sh1 (Clone ID: V2THS_230143) and pTRIPZ SETD7 sh2 (Clone ID: V2THS_99174)—were purchased from Dharmacon and Sigma-Aldrich. The HEK293T cells were plated in 10 cm dish and transfected with target plasmid and packaging plasmids (pMD2G and pPAX2) using Lipofectamine 2000 according to the manufacturer's protocol (Life technologies; 11668019). The transfected HEK293T cells incubated for 3 days and medium was collected every day. Collected medium was centrifuged at 3000 g for 15 min to remove cells and cell debris. Supernatant containing virus was concentrated by PEG-it virus concentrator solution according to the manufacturer's protocol (System Bioscience; LV810A). H7 or HES3^{NKX2-5eGFP/w} hESCs were seeded onto 6-well plates and infected with lentivirus containing the shRNA for SETD7. Cells expressing control or SETD7 shRNA were selected by puromycin (2 µg/ml) treatment for 2-3 days.

METHOD DETAILS**Differentiation of human PSCs to CMs**

For cardiac differentiation, a chemically defined monolayer differentiation protocol was used as previously described ([Ebert et al., 2014; Wu et al., 2015](#)). Briefly, iPSCs at ~90% confluence were incubated with differentiation basal medium comprising RPMI 1640 medium (Invitrogen) and B27 supplement minus insulin (Invitrogen). CHIR99021, a selective glycogen synthase kinase

3β inhibitor, was added to the differentiation basal medium. On day 2, medium was removed and replaced with differentiation basal medium minus CHIR99021. On day 3, the Wnt antagonist, IWR-1, was added to the medium. After 48 hr, medium was removed and replaced with differentiation basal medium without any inhibitors. On day 7, the cells were incubated with complete CM medium consisting of RPMI 1640 medium and B27 supplement plus insulin (Invitrogen). The medium was changed every 2 days. Monolayers of CMs derived from iPSCs (iPSC-CMs) were cultured for ~30 days and subsequently dissociated for experimental use using TrypLE Express (Life Technologies). Specific day time point of selected four different stages are day 0 (hESC), day 2 (MES), day 5 (CP), day 9 (CM), and day 30~40 (purified CM).

Immunoblotting and immunoprecipitation

For immunoblotting, each sample was subjected to electrophoresis on 4%–12% NuPAGE Bis-Tris gradient gels (Life Technology; NP0335) and proteins were transferred to polyvinylidene difluoride membranes using wet-based transfer system (Bio-Rad). Membranes were incubated overnight with the indicated primary antibodies, followed by incubation for 1 hr with horseradish peroxidase-conjugated secondary antibody (Abcam; ab131366). Signals were detected by chemiluminescence. For immunoprecipitation, cells were harvested and lysed in IP lysis buffer (Thermo Scientific; 87788). Lysates were centrifuged for 10 min at 10,000 g at 4°C. Specific antibodies conjugated with magnetic protein G beads (Life Technology; 10004D) (or agarose beads (Active Motif; 53039)) were added to supernatants for overnight incubation at 4°C. Subsequently, beads were pelleted for 1 min at 7,000 rpm and washed twice with IP lysis buffer. Proteins were eluted in 2 × Laemmli buffer (Bio-Rad) or 4 × LDS sample buffer (Life Technology; NP0007) by boiling for 10 min. Immunoprecipitated proteins were subjected to immunoblotting using horseradish peroxidase-conjugated primary antibodies or VeriBlot of IP Detection Reagent (Abcam; ab131366).

RNA extraction and quantitative real-time polymerase chain reaction (qRT-PCR)

Total RNA was isolated using RNeasy Plus Mini Kit or miRNeasy Mini Kit (QIAGEN; 74134, 217004). Reverse transcription was performed using iScript cDNA Synthesis Kit (Bio-Rad; 1708890) and qRT-PCR was performed using iQ® SYBR Green Supermix (Bio-Rad; 170-8880) or TaqMan® Universal PCR Master Mix (Applied Biosystems; 4304437) on CFX96 real-time PCR detector (Bio-Rad). Relative mRNA levels were normalized to those of 18S or GAPDH mRNA in each reaction. Three or Four biological replicates per group were used for qRT-PCR.

Chromatin immunoprecipitation and ChIP-seq

Antibodies were used as described above. Each antibody was incubated with Dynabeads (Life Technology; 10003D) for 12 hr at 4°C. A small portion of the crosslinked, sheared chromatin was saved as Input and the remainder was employed for the immunoprecipitation using antibody conjugated Dynabeads. After overnight incubation at 4°C, incubated beads were rinsed with sonication buffer (50 mM HEPES pH 7.9, 140 mM NaCl, 1 mM EDTA, 1% Triton X-100, 0.1% Na-deoxycholate, 0.1% SDS, 0.5 mM PMSF), high salt buffer (50 mM HEPES pH 7.9 500 mM NaCl, 1 mM EDTA, 1% Triton X-100, 0.1% Na-deoxycholate, 0.1% SDS, 0.5 mM PMSF) and LiCl buffer (20 mM Tris, pH 8.0, 1 mM EDTA, 250 mM LiCl, 0.5% NP-40, 0.5% Na-deoxycholate, 0.5 mM PMSF). Washed beads were incubated with elution buffer (50 mM Tris, pH 8.0, 1 mM EDTA, 1% SDS, 50 mM NaHCO₃) for 1 hr at 65°C and de-crosslinked with 5 M NaCl for overnight at 65°C. Immunoprecipitated DNA was treated with Rnase A and Proteinase K and purified by ChIP DNA clean and concentrator (Zymo Research; D5205).

Intracellular calcium imaging

Single iPSC-CMs were plated onto Matrigel-coated coverglass (CS-24/50, Warner Instruments, Inc.) at a density of ~10,000 cells per square centimeter. Cells were allowed to recover for 3–4 days and loaded with 5 μ M Fura-2 AM (Thermo Fisher Scientific) in Tyrode's solution (140 mM NaCl, 5.4 mM KCl, 1 mM MgCl₂, 10 mM glucose, 1.8 mM CaCl₂, and 10 mM HEPES, pH adjusted to 7.4 with NaOH at room temperature) for 30 min at room temperature. Cells were imaged on a customized Ti-S/L 100 Inverted Microscope based imaging platform with 40x oil immersion objective (CFI SUPER FLUOR, NA 1.30 WD 0.22). Bipolar pulse was used to pace cells at 0.5 and 1 Hz. Cells were kept at 37°C while recording. Fura-2 signals were captured in high frame rate video recording mode (512 × 512 pixels) at a speed of 50 frames per second. Videos were analyzed with NIS Elements: Advanced Research Software (Nikon) and raw ratio-pair data were further processed with custom-made script based on Interactive Digital Language.

Immunofluorescence staining and confocal microscopy

hESC-CMs were fixed in 4% paraformaldehyde in phosphate buffered saline. Following permeabilization with 0.3% Triton X-100, CMs were stained with primary antibodies against cardiac troponin T type 2 (TNNT2; Thermo Scientific and Abcam) and SETD7 (Abcam). After reaction with the primary antibodies, cells were incubated with the appropriate Alexa Fluor-conjugated secondary antibodies (Santa Cruz Biotechnology or Life Technologies). Images of the stained cells were obtained under a brightfield microscope (Leica). Confocal images were taken by using a 63 × Plan-Apochromat oil immersion objective (Carl Zeiss) and a LSM 510 Meta confocal microscope (Carl Zeiss). Images were analyzed by using ZEN software (Carl Zeiss) and ImageJ software (National Institutes of Health).

QUANTIFICATION AND STATISTICAL ANALYSIS

Statistical analyses for each experiment are described in the figure legends or in the appropriate text. Multiple group comparisons were calculated using one-way ANOVA. Pairwise comparisons were carried out using the two-tailed unpaired Student's t test. * $p < 0.05$; ** $p < 0.01$; *** $p < 0.005$. All error bars are defined as SEM unless indicated.

Chromatin immunoprecipitation and ChIP-seq analysis

ChIP-seq data were aligned to the human genome (hg19) or mouse genome (mm10) by Bowtie (<http://bowtie-bio.sourceforge.net/index.shtml>) with only uniquely aligned reads kept. All duplicate reads were removed by SAMtools (<http://www.htslib.org/>). FastQC was applied for quality control of sequencing (<http://www.bioinformatics.babraham.ac.uk/projects/fastqc/>). PhantomPeak was applied for quality control of ChIP-seq (<https://code.google.com/archive/p/phantompeakqualtools/>). For all samples generated, normalized strand coefficient (NSC) was above 1.05 and relative strand correlation (RSC) was above 0.8. The aforementioned pre-processing scripts are available online (https://github.com/ny-shao/chip-seq_preprocess). The genebody annotations of protein coding genes were extracted from ENSEMBL V75 and bedtools were applied to extract the aligned reads in genebody regions for all ChIP-seq samples (<http://bedtools.readthedocs.io/en/latest>). The counts tables of SETD7 and the histone marks of coding genes were fed to DESeq for estimation of fold changes of reads enrichment in time series and genes with significant enrichment changes (adjusted P -value < 0.1 , fold-change > 2) in pairwise comparisons were selected for downstream analyses (<http://bioconductor.org/packages/release/bioc/html/DESeq.html>). Fold changes were clustered by K-means ($k = 5$) clustering in R. Functional enrichment analyses were implemented by GeneAnswer package of Bioconductor (<https://www.bioconductor.org/packages/release/bioc/html/GeneAnswers.html>). Gene regulatory network was generated by iRegulon package (<http://iregulon.aertslab.org/>) in Cytoscape (<http://www.cytoscape.org/>). Average profile and heatmaps of the genomic features of ChIP-seq were generated by ngs.plot (<https://github.com/shenlab-sinai/ngsplot>) (Shen et al., 2014). Orthologs of human and mouse were downloaded from Mouse Genome Informatics (MGI, <http://www.informatics.jax.org/homology.shtml>) and genes were sorted based on the enrichment density of SETD7 calculated by ngs.plot normalized to reads per millions. The tracks screenshots of sequencing data were generated by IGV browser (<https://www.broadinstitute.org/igv/>). Corrgram package in R software was used to calculate and visualize correlation among different chromatin remodelers and histone marks.

RNA-seq analysis

RNA-seq data generated by Illumina sequencer were assembled by STAR (<https://github.com/alexdobin/STAR>) to the human genome (hg19). The Ampliseq data were processed by Ion Torrent server. The transcriptome annotation was downloaded from GENCODE project (V19) (<http://www.gencodegenes.org/>). Fold changes of expression levels were estimated by DESeq as aforementioned in ChIP-seq analyses. Functional enrichment analyses were implemented by GeneAnswers package.

DATA AND SOFTWARE AVAILABILITY

The accession number for the RNA-seq and ChIP-seq data reported in this paper is GEO: GSE107785.